CHAPTER 3

PLASMA POLYMERIZATION

3. PLASMA POLYMERIZATION

3.1 INTRODUCTION

The plasma work developed during this thesis has been focus on the nucleation and growth process in plasma polymerization and the electrical properties of plasma-polymerized organic thin films. Related to this, the formation of thin polymer films by means of a glow discharge in the vapour of a monomer at low pressure, what is known as plasma polymerization, has been well known for many years.[1] It should be noted that some authors do distinguish between the terms plasma polymerization and glow discharge polymerization, even luminous chemical vapour deposition is becoming a quite common term in the last years. Since it could be misleading, no differences will be done in this work among them.

In the 1960s, there was an increasing interest in using polymerized thin films in the microelectronic research and industry. Due to the high electrical resistance that presented some of them, one of the first applications for these glow discharged polymerized thin films was using them as possible dielectric materials.[2,3] The monomers which were employed included acetylene, naphthalene, styrene and certain metalorganics, such as ferrocene or diphenyl mercury. Nowadays, the use of polymerized thin films with low dielectric constants for microelectronics has gained a lot of attention, especially due to the continue decreasing size of the electronic components, the state of the art on this theme can be found in literature.[4]

Nonetheless, the research in these polymerized thin films has not been only addressed towards dielectric applications. Thin films are applied in a wide range of applications. Plasma polymerized fluorocarbon films are used as packaging materials due to their hydrophobic properties.[5] Plasma polymerized thiophene thin films are excellent candidates to be used as organic semiconductors for transistor applications.[6] Additionally, despite its insulators properties, polymers can behave as conducting materials. Xie *et al.* processed a conducting plasma film using tetracyanoquinodimethane with quinoline.[7] Within this area, the developing of sensors arrays has become an important target for a lot of researcher groups. The main efforts have been focused on chemical sensors[8] and biosensors arrays.[9] In this sense, part of

the work is related to the synthesis of conducting polymeric thin films for these applications.

In this chapter, the deposition process and the thin film formation of PPy have been described. In the first part, the nucleation-growth mechanism has been investigated on the different substrates. In the second part, characteristics and methods to achieve the conducting PPy films have been depicted.

3.2 EQUIPMENT AND METHODS

In this chapter, the study of PPy deposition and doping process is based on surface characterization techniques. Most of them have been employed in every section and therefore this section compiles all the techniques, which are depicted next:

AFM images were acquired with two different microscopes: Nanoscope III Extended Multimode Atomic Force Microscope (Digital Instruments, Santa Barbara, CA), with lateral resolution of 5 nm and vertical of 1 Å, by tapping mode; and XE-100 (PSIA Inc.) with lateral resolution of 0.15 nm and vertical of 0.05 nm, by non-contact mode. Images were analyzed by the Nanoscope III v4.22 software for Nanoscope microscope; and by XEP and XEI software for data acquisition and image processing respectively for the XE-100 microscope.

Contact angle was determined by KSV CAM 200 goniometer, using milli-Q water and KSV OTD "One touch dispenser" to obtain each drop, and they were recorded by the KSV CAM software.

TOF-SIMS analysis was performed using a TOF-SIMS IV mass spectrometer (ION-TOF, Munster, Germany) operated at a pressure of 5×10^{-9} mbar, 18 ns pulses of 25 keV Bi^{3+} (primary ions) were bunched, with an incidence angle of 45º, to form ion packets with a nominal temporal extent of <0.9 ns at a repetition rate of 10 kHz, which produced a target current of 0.2 pA. These primary ion conditions were used to scan a 125x125 μm area of the sample for 30 s.

Fourier transform infrared (FT-IR) measurements were performed on a Nicolet Nexus 870 ESP spectrometer in normal transmission mode equipped with a MCT (mercury cadmium tellurium detector and KBr beamsplitter. Spectra were acquired over the range of 400 to 4000 cm^{-1} with a 4 cm^{-1} resolution for 256 scans. All spectra were baseline-corrected.

Samples thickness was measured via dynamic spectroscopic ellipsometry (M-2000, J.A. Woollam). All data were collected at a 75º incident angle for 220 wavelengths between 313 and 718 nm and fit to a Cauchy–Urbach isotropic model with an ambient water layer using commercial modeling software (WVASE32, J.A. Woollam). This model fit the refractive index (as a function of wavelength) and the film thickness to the experimental data. FT-IR and ellipsometry characterization were performed using silicon wafers as substrate.

Photoelectron spectra of the monolayers were recorded at a 35⁰ take-off angle relative to the substrate surface with a SSX-100 spectrometer using the monochromatized X-ray Al Kα radiation (1486.6 eV). Nominal resolution was measured as full width at half-maximum of 1.0 (core-level spectrum) to 1.5 (survey spectrum). The analysed core-level lines were calibrated against the C 1s binding energy set at 285 eV, characteristic of alkyl moieties. The acquired signals were analysed using mixed Gaussian-Lorentzian curves (80%-20% respectively).

Scanning electron microscopy (JEOL JSM-5310 SEM with microanalysis Oxford Inca Energy) was carried out to study the adherence test results.

The standard test method for measuring adhesion by tape test (ASTM D3359) was done as follows. Using a metallic knife with a cutter spacing of 1 mm, adapted for coating thickness less than 60 μm (Elcometer 1542 Cross Hatch Adhesion Tester), a cut was made of approximately 30 mm long ensuring that enough force is used to cut all the way down to the substrate. Another set of parallel cuts were made perpendicular to the first set and of a similar length, ensuring that the cut is all the way down to the substrate, again. The surface was slightly brushed with a soft brush to remove any detached flakes or ribbons of coating. Then, a 3M 4-9239 tape was applied on the cut area and removed slowly in order to evaluate the coating-substrate adherence.

3.3 PLASMA REACTOR

The plasma reactor consisted of a stainless steel round vessel (49 cm-diameter, 42.5 cm-length) parallel plate reactor (Figure 1). It was capacitively coupled to a 13.56 MHz radiofrequency power supply through a matching network. The radiofrequency electrode was a stainless steel plate, located in the middle of the reactor approximately, and the ground electrode was the internal side of the reactor chamber. Samples were placed in the radiofrequency electrode in a fixed position near the edge.
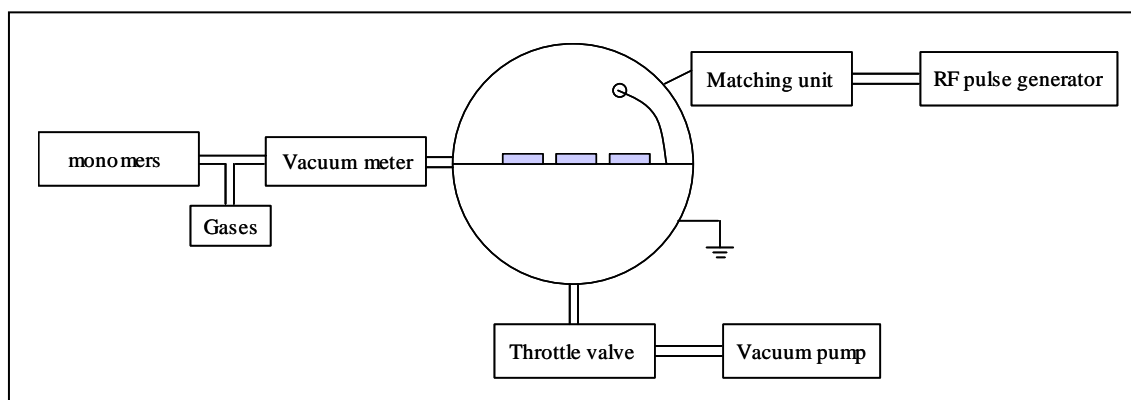

Figure 1. Scheme of the plasma reactor chamber.

The reactor chamber was evacuated by a two-stage rotatory vane vacuum pump (TRIVAC D 16 BCS-PFPE, Oerlikon Leybold Vacuum) and a cold trap was placed between them to protect the vacuum pump. The system pressure was determined using a Pirani type vacuum meter (MKS), positioned between the reactor and the cold trap. The monomer was supplied to the chamber via manifold with gas fluxes adjusted with needle valves.

Figure 2. Image of the plasma reactor.

3.4 NUCLEATION AND GROWTH OF PLASMA POLYMERIZED POLYPYRROLE

3.4.1 INTRODUCTION

This part of the thesis is one of the most important as it can supply valuable information in one field which has not been studied deeply. As it has been commented before, there have been numerous investigations reporting the deposition and polymerization of polypyrrole on substrates modified with a monolayer by electrochemical techniques. They have discussed about the role of the monolayer in this process and how the pyrrolitic terminal group enhances the deposition. Because of this, the investigation of the monolayer effect but using plasma polymerization as the deposition technique can be a very challenging option and it can contribute to a better understanding of the process. To our knowledge no similar researches had been done until now in this area. Moreover, we have tried to go a step beyond and to study the nucleation process since its first stage. It has been possible to determine the role of the monolayer in the plasma polymerization by analyzing the very early instants of PPy deposition. The use of AFM or TOF-SIMS, among other characterization techniques, has given unquestionable evidences of the advantages of using a pyrrole-terminated monolayer as nucleation promoter.

This study is focused on the nucleation and growth of PPY during the deposition. Because of that, a schematic representation of the rapid step growth polymerization mechanism in the luminous gas phase is presented in Figure 3.[10] Summarizing, when the monomer is exposed to the luminous phase it yields chemically reactive species. These species can be recombined with another reactive specie or with another monomer to start again the cycle and continue with the chain growth polymerization or they can be deposited on the substrate. It should be commented that the reactive species are represented by free radicals as they are the species most commonly created, but other reactive species, such as ions, can participate in the mechanism.
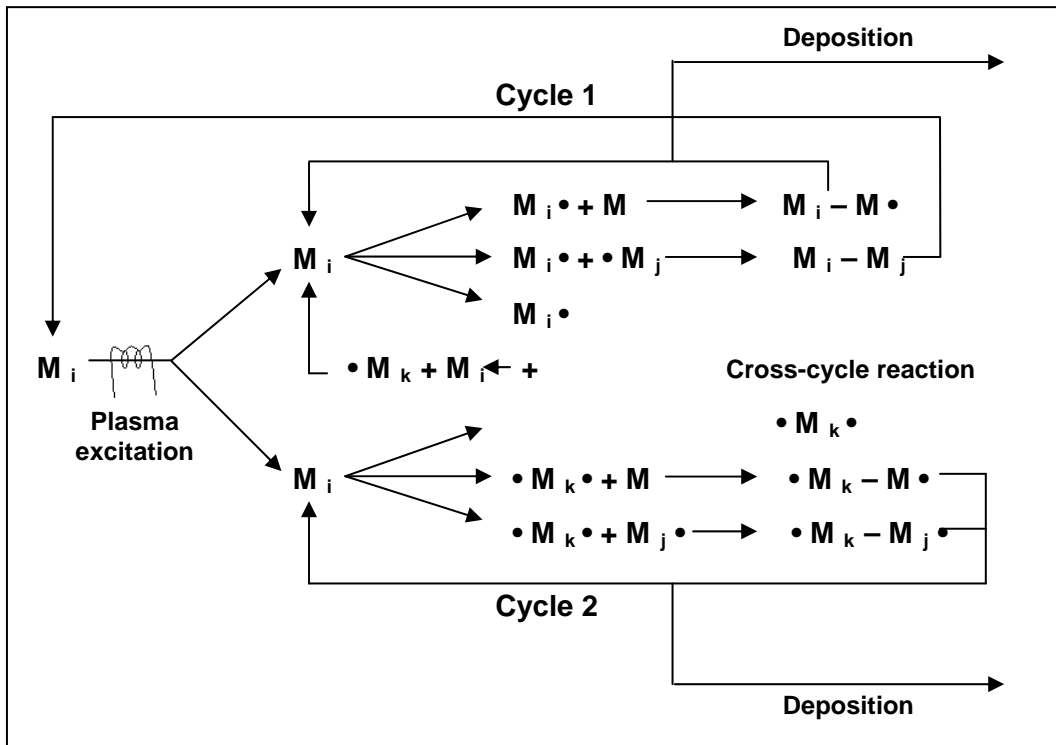
Figure 3. Rapid Step-Growth Polymerization and deposition mechanism in the luminous gas phase.

Previous studies performed by Borrós[11] and Martin[12] about plasma polymer deposition have been used to choose the experimental conditions employed in the first experiments. These works deal with several plasma parameters, such as power or duty cycle, in order to study the nucleation, growth, structure and morphology of conducting polymers. For instance, the power peak was set at low values in order to obtain uniform films and to avoid aromatic cycle breaking due to the discharge. Moreover, these studies suggest the use of pulsed plasma conditions to obtain more uniform films.

Related to this, the employment of pulsed plasma has been totally accepted as an excellent technique to control film chemistry during plasma deposition.[13] The modulation of the pulsed plasma is defined by the Duty Cycle (DC), which is the relationship between the fraction of time that the system is in an active state, that is, when the plasma is on (t_{ON}), and the total pulse duration ($t_{ON} + t_{OFF}$) (Equation 1).

$$DC = \frac{t_{ON}}{t_{ON} + t_{OFF}} \tag{1}$$

Therefore, the resulting power (equivalent power, P_{eq}) is proportional to the modulation of the duty cycle.

$$P_{eq} = P_{peak} \times DC \qquad\qquad (2)$$

During the t_{ON} the reactive species are generated and the nuclei are formed preferably. The more time the plasma is on, the more reactive species are generated. While in the t_{OFF}, the polymer growth occurs preferably. During this period, both monomers and remaining reactive species can react to enhance the nuclei growth. Furthermore, the t_{OFF} reduces the monomer fragmentation and the ion bombardment on the surface, which increases the retention of the film functionality.

One of the most important aims in this investigation is to study the relevance of the pyrrole group in ω-(N-pyrrolyl)alkane monolayers for the PPy deposition by PECVD. Particularly interesting were the results obtained by McCarley research's group, in which they discovered that a pyrrole-terminated monolayer enhanced the PPy nucleation on the surface by electrochemistry polymerization.[14,15] In this section, the idea is to demonstrate that this effect can be extrapolated to PECVD techniques.

Plasma polymerization consists of activation of the starting material (monomer) by the interaction of gas phase molecules with plasma, then, the product is deposited on the substrate. The nucleation step involves the absorption of these first aggregates on the surface to form a film. Additionally, the chain growth occurs via polymerization of adsorbed monomer on the surface. Thus, the critical point for the plasma polymer formation is nucleation. In other words, the interaction between activated species and the substrate plays an important role in the polymerization mechanism. The lesser interactions, the lesser nuclei formed and, as a consequence, more difficulty to achieve a polymer layer. In this sense, AFM can contribute to get valuable information about the deposition and growth-chain processes. AFM is a very powerful tool to study the topography surface at the nanometer scale. This technique enables to work with a very low deposition range and to observe the polymer deposition at its first stage.

3.4.2 EXPERIMENTAL PART

The experimental conditions for the nucleation and growth study were fixed for the three different surfaces employed.

The reactor chamber was evacuated to a base pressure of 0.04 mbar and the working pressure was set at 0.08 mbar during pyrrole deposition. All polymerizations were performed under pulsed plasma. The pulsed RF power setting was 20 W, with a 90% duty cycle and a frequency of 15 Hz. Polymerization times varied from 1 to 5 min.

3.4.3 PLASMA POLYMERIZATION ON GOLD SURFACES

3.4.3.1 Atomic Force Microscopy

In every reaction a bare gold surface, a Py3SH SAM and a Py12SH SAM-modified gold surface were introduced into the reactor chamber at the same time to compare the effect of plasma polymerization under the same conditions. The PPy nucleation and growth on the different substrates have been studied to give evidence of the differences between unmodified and SAM-modified gold surfaces, as well as, the difference between shorter and longer alkyl chains in SAMs.
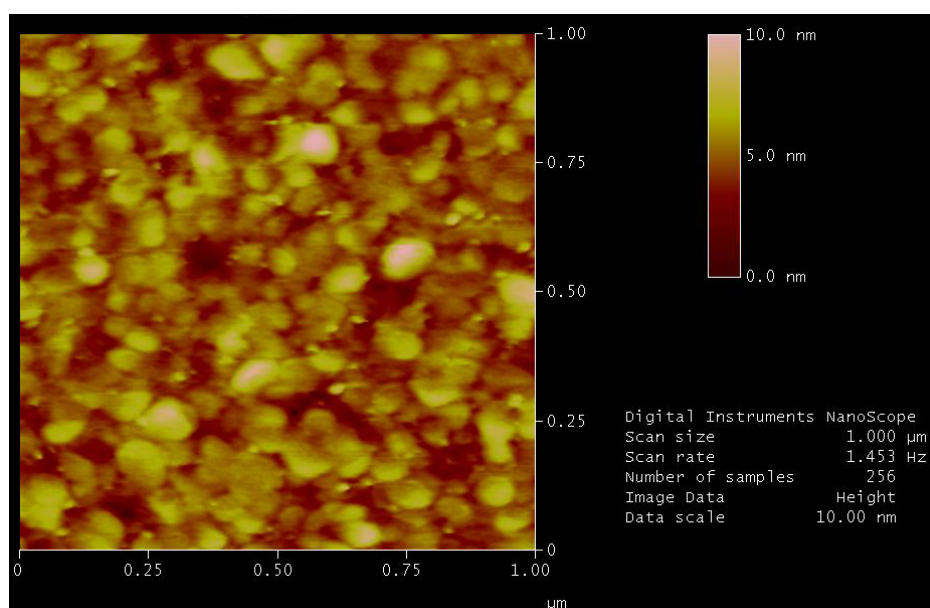

Figure 4. AFM image of a bare gold surface.

The surface topography of bare gold substrate was characterized by AFM since all the polymerizations were performed on gold surfaces. When the gold covering is deposited by thermal evaporation, it leaves a very characteristic surface. Gold growth is island-like, which has been studied for spectroscopic and sensing applications.[16,17] Figure 4 displays the characteristic topography of an evaporated gold film. Gold accumulations are what are known as islands, mainly because of their shape. Furthermore, AFM images of different SAM-modified gold surfaces were acquired as well. An example can be observed in Figure 5, which presents the gold surface modified by a Py12SH SAM. As it can be seen, there are no significant differences between the modified and unmodified gold surface. In Figure 5, the same island-like topography was obtained on the surface. Therefore, it means that the SAM can not be detected with the resolution employed. To obtain the monolayer structure it would be required an STM analysis, which can provide a better study about the SAM. For instance, Bumm *et al* used STM to image adjacent chains and molecular terraces of different length alkanethiolates in an ordered SAM lattice in Au {111}.[18] Another important factor related to the gold landscape is the surface roughness (~5 nm), which makes the observation of SAMs quite difficult or even impossible due to monolayer chain length (between 7 and 20 Å, approximately).
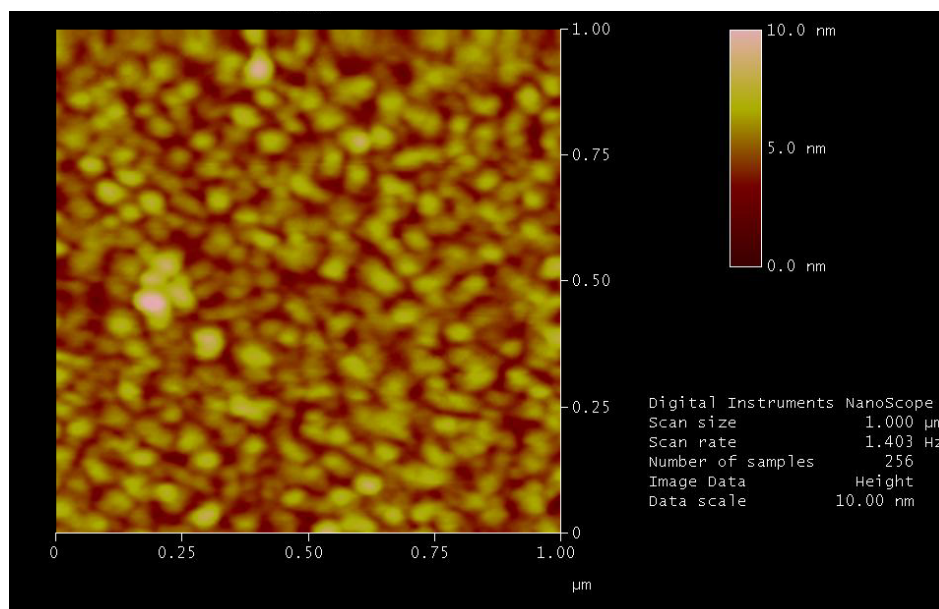

Figure 5. AFM image of a Py12SH SAM on a gold surface.

More interesting are Figure 6, Figure 7 and Figure 9 which show the surfaces after different times of polymerization. At 2 minutes of plasma polymerization (Figure 6), the first PPy nuclei were detected by AFM. The white dots, that appear spread over the

surface, correspond to these nuclei. On the gold surface, just a few nuclei have been deposited (Figure 6-A). In contrary, Figure 6-B and C show a larger number of PPy nuclei presenting a bigger size. At this point, the experiment gives evidence that the monolayer has a positive effect on the PPy nucleation. It seems that the pyrrole terminated group enhances the deposition from the vapour phase. Probably, the similarity between the terminal pyrrole ring in the SAM and the activated species in the luminous phase favours the deposition on the monolayer. Moreover, there is another factor that needs to be taken in account, which is the surface activation. When the plasma is on, not only it can activate the pyrrole in the vapour phase, but the pyrrole ring in the SAM can be activated as well. Thus, the formation of radicals in the pyrrole group can initiate the polymerization by reacting with adsorbed monomers, what is known as grafting polymerization. This can be another way of improving nucleation on the surface.
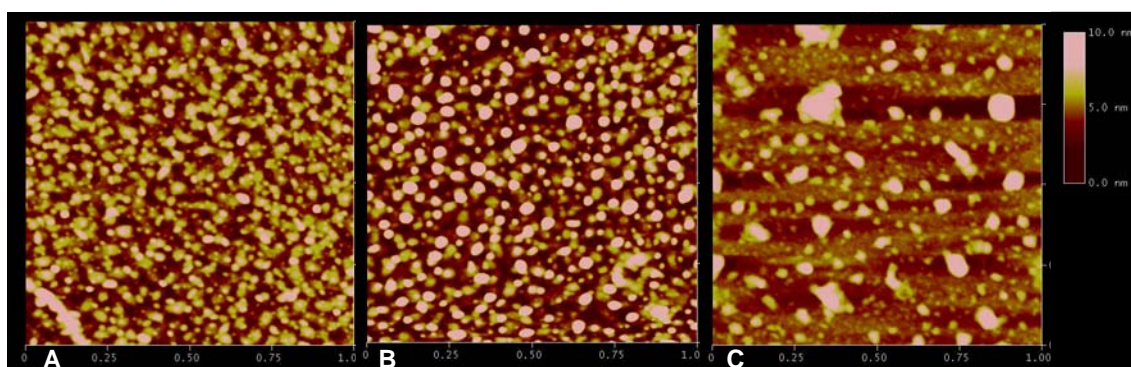

Figure 6. AFM images of bare gold (A), Py3SH SAM (B) and Py12SH SAM (C) polymerized for 2 minutes.

Another finding is the difference between nuclei on Py3SH and Py12SH SAMs. Nuclei on Py3SH are smaller and with very similar size, while on Py12SH nuclei are quite bigger and with different size. These differences can be explained by the preferential growth of PPy nuclei on the Py12SH monolayer. It could be assumed that some domains on the surface are better structured due to the longest alkyl chain and it enhances the PPy growth.
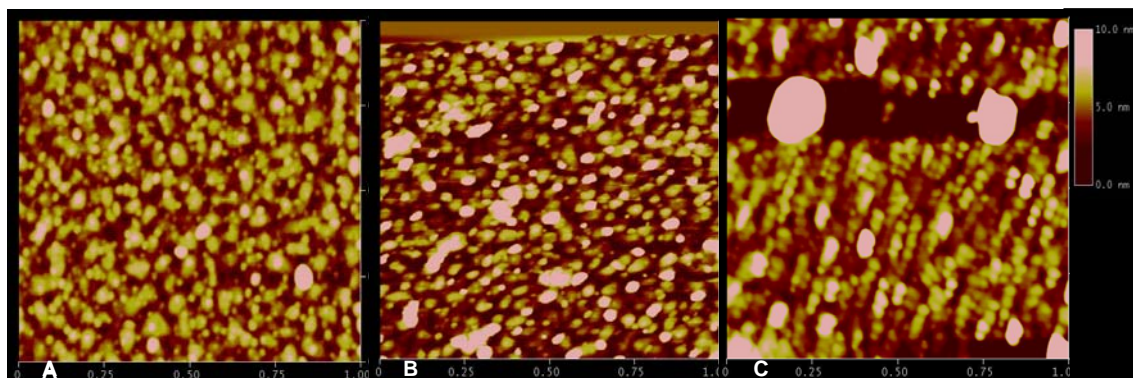
Figure 7. AFM images of bare gold (A), Py3SH SAM (B) and Py12SH SAM (C) polymerized for 3.5 minutes.

No important differences have been observed in samples polymerized for 3.5 minutes (Figure 7) in comparison with the ones at 2 minutes. There are barely some nuclei on the unmodified gold surface, whereas on SAM-modified surfaces there are plenty of them. Nevertheless, taking a look at the 3-D AFM images of Py3SH and Py12SH surfaces (Figure 8) some different characteristics can be observed. Nuclei on Py12SH are higher than those on Py3SH and more PPy has been deposited on the Py12SH monolayer as well. The AFM images support the idea that better structured monolayers act as better nucleation sites, probably because of a better orientation of the pyrrole group.
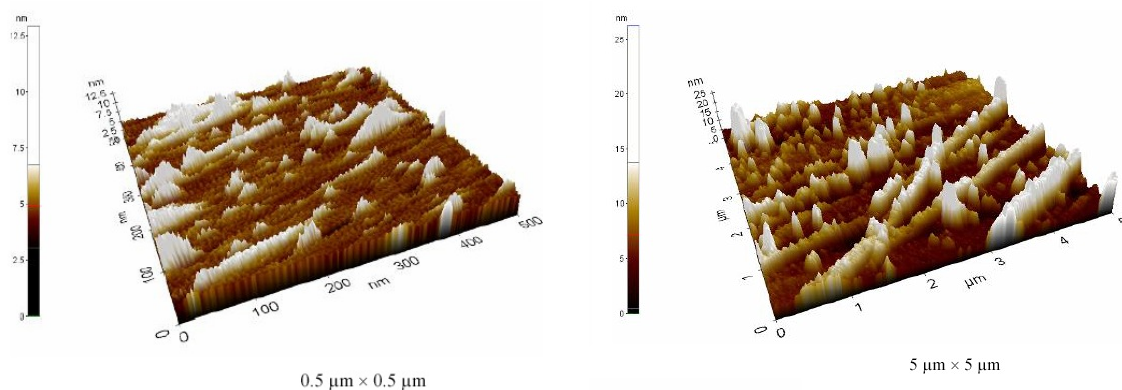

$0.5 \ \mu m \times 0.5 \ \mu m$

$5 \ \mu m \times 5 \ \mu m$

Figure 8. 3-D AFM images of Py3SH and Py12SH SAMs on gold polymerized for 3.5 minutes.
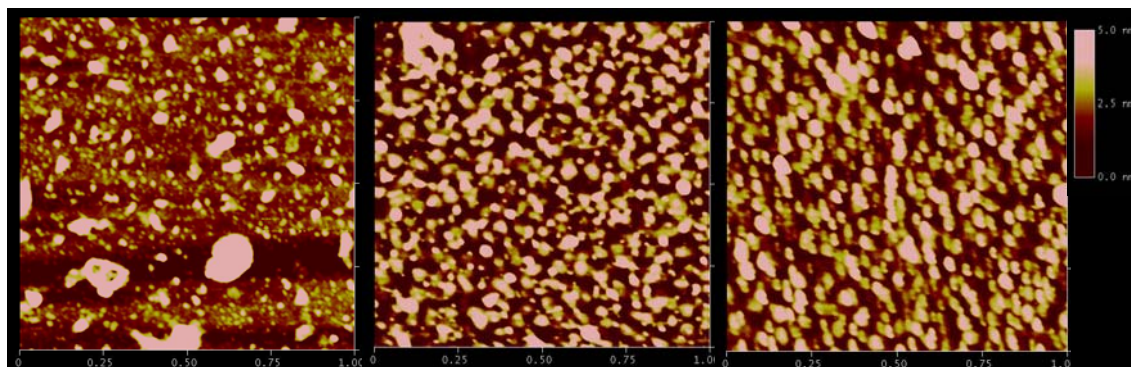
Figure 9. AFM images of unmodified gold (A), Py3SH SAM (B) and Py12SH SAM (C) polymerized for 5 minutes.

Finally, Figure 9 shows AFM images of unmodified gold, Py3SH and Py12SH SAM-modified surfaces polymerized for 5 minutes. The unmodified gold substrate (Figure 9-A) displays several nuclei on the surface, which were not observed in previous polymerizations. Figure 9-B and C, corresponding to Py3SH and Py12SH monolayers, present a very similar topography. The entire surface is covered by PPy aggregates, represented by the white dots, which have approximately the same size. At 5 minutes of plasma polymerization a PPy film has been synthesized in both SAM-modified surfaces. The nuclei are deposited everywhere regardless preference zones due to the surface homogeneity of the first PPy layer, which acts as a nucleation site for further polymerization. This is the reason why nuclei have the same size and they can grow without any preferences in comparison with the unmodified gold surface which shows a quite irregular topography. Film thickness was of 50 nm for the Py12SH sample and 35 nm for the Py3SH substrate.

3.4.3.2 Contact angle

Water contact angle measurements were performed to study the hydrophilic or hydrophobic character of SAM-modified surfaces at different polymerization times. In addition, the water contact angle for both monolayers was measured as well. Py3SH monolayer has a contact angle of 55.5⁰, which is very similar to the gold surface contact angle (56⁰). At first, it would be logical to think that it is not possible to observe the monolayer effect on the surface wettability due to a bad structuration and that the measure corresponds to the gold surface contact angle indeed. However, Willicut[14] reported that SAMs of ω-(N-pyrrolyl)alkanethiol with chain lengths of 3, 5 and 6 methylenes had a contact angle of 58⁰, which is quite close to the value obtained experimentally. Because of this, it can be assumed that the assembly and formation of

ω-(N-pyrrolyl)alkanethiol monolayers has been achieved, in spite of having the same contact angle than the gold surface.

Water contact angle for Py12SH SAMs is 60.6º, a little bit minor to the one found in recent literature which was of 65º.[19] The higher contact angle for the Py12SH in comparison with the Py3SH suggests a more compact monolayer for ω-(N-pyrrolyl)alkanethiols with a longer alkyl chain. The increase of Van der Waals interactions among methylenes in the Py12SH SAM leads to a better ordering. This order does affect to the terminated group too. Thus, the change in contact angle is due to the effect of the pyrrole group and its orientation (see Chapter 2).

Table 1. Contact angle measured on SAM-modified gold surfaces at different times of plasma polymerization.

	Polymerization time (min)			
	0	1	2	5
Py3SH	55.5	38.0	42.8	52.1
Py12SH	60.6	42.0	47.1	57.2

A drastically contact angle decreased can be observed for samples polymerized for 1 minute. At this time, residual oxygen and nitrogen remaining in the plasma polymerization chamber may interact with plasma leading to the formation of hydroxyl (-OH), carbonyl (-CO-), carboxyl (-COO-), amine (-NH$_2$) and amide (-CONH$_2$) groups on the surface. Thus, because of their polar character, the hydrophilicity increases. At 2 minutes, coinciding with the time at which nuclei were observed by AFM, water contact angle increased, probably due to the PPy deposition. Once a PPy film was deposited on the monolayers at 5 minutes of plasma polymerization, the contact water angle was of 52.1 and 57.2º for Py3SH and Py12SH SAMs. Cen *et al*[20] reported a 68º contact angle for electrochemical synthesis of PPy films and Ooij *et al*[21] measured a contact angle of 66º for plasma polymerized pyrrole films. The values obtained in this work were lower than these ones. It was owed to the fact that plasma polymerization leads to a product different to the one obtained by electrochemical synthesis and that different plasma conditions lead to polymers with different composition.

3.4.4 PLASMA POLYMERIZATION ON COPPER SURFACES

3.4.4.1 Atomic Force Microscopy

The deposition process is studied by AFM again in order to determine the influence of the monolayer in the nucleation-growth step on unmodified copper and SAM-modified copper substrates. Samples were polymerized in the same batch process to compare their topography among them.

Figure 10 shows the surface topography of bare copper. Topographic features can be attributed to the polishing process. This image can be taken as a reference for further discussion about the polymerization process. SAM-modified copper AFM images have not been included as no differences were observed among them and the copper substrate. Neither a domain nor an orientation on the surface can be observed, probably due to the AFM resolution and the copper roughness (10 nm).
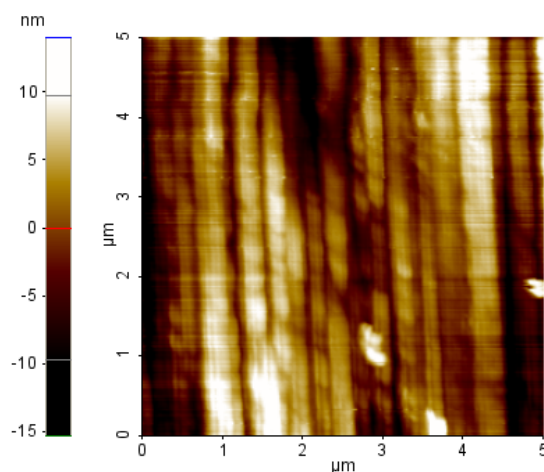

Figure 10. AFM image of a bare copper substrate.

AFM images of different samples at different polymerization times are presented in Figure 11. The white dots in images represent the PPy nuclei deposited on the surfaces. At 2 minutes, the first stage of the polymerization is observed. At image 19-1, corresponding to unmodified copper substrate polymerized for 2 minutes, some tiny PPy nuclei are detected, as described before for gold surfaces. In contrast, in Py12SH and Py12SeH samples, images 19-3 and 19-5 respectively, present more and bigger nuclei on the surface. These images indicate that the pyrrole moiety in SAMs act as a nucleation site. The pyrrole group enhances the deposition from the vapour phase of the activated specie. This can be due to the similarity between both species. What is important to note is that bigger nuclei shown in SAM-modified copper samples have

been formed by the growth of preexisting nuclei in such a way that these PPy nuclei increase their size until covering the entire surface. This interaction shows the process by which the PPy layer is achieved.
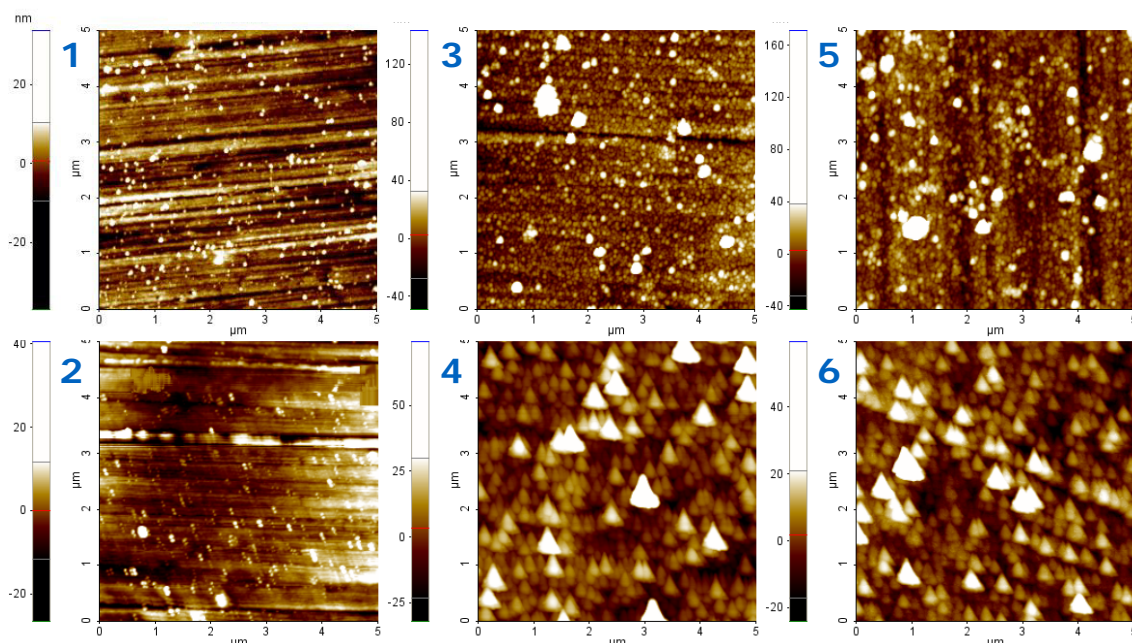

Figure 11. AFM images for 2 and 5 min of plasma polymerization on bare copper (1, 2), on Py12SH (3, 4) and on Py12SeH (5, 6).

Besides, samples polymerized for 5 minutes are shown as well, in order to compare with the ones polymerized for 2 minutes. Bare copper polymerized for 5 minutes (Image 19-2) presents a very similar topography to that obtained after 2 minutes of polymerization. There are only a few nuclei spread over the surface and their size has not increased considerably with regard to nuclei at 2 minutes. In general, it seems that after 5 minutes of polymerization the deposition on unmodified substrates has not been improved and the nuclei growth is not achieved efficiently. This image contrast with those of Py12SH and Py12SeH monolayers polymerized for 5 minutes (Image 19-4 and 19-6). SAM-modified surfaces topography is clearly different to unmodified copper. Nuclei size is quite bigger and they can be found everywhere on the surface, which suggest that a PPy thin film has been synthesized.

It should be noticed that no differences are observed for thiol or selenol SAMs related to size and shape of nuclei, the plasma polymerized surfaces are practically undistinguishable. Since both monolayers present a similar quality (see 2.2.3), these finding suggest that the anchoring group does not influence on the polymer deposition. Moreover, AFM images show a homogeneous growth for both monolayers. This means

that, initially, nuclei grow until a first layer is formed and then, nuclei continue depositing on it to form a PPy film. Therefore, it has been demonstrated the effect of the monolayer in the deposition and growth of PPy on copper. The surface modification has lead to an enhancement in the nuclei formation and the posterior growth to obtain a thin film.

3.4.5 PLASMA POLYMERIZATION ON SILICON WAFERS

3.4.5.1 Atomic Force Microscopy

The surface topography and morphology for the deposition process was again studied by AFM. The AFM image of a bare silicon wafer is shown in Figure 12 (RMS roughness of 0.23 nm). Figure 13, Figure 14 and Figure 15 displays the topography of silicon wafers and Py11Si-modified silicon wafers at different polymerization times (1, 2 and 5 minutes, respectively). At 1 minute of plasma polymerization, there are PPy nuclei deposited onto both surfaces, but it is on the SAM-modified surface where bigger nuclei are found.
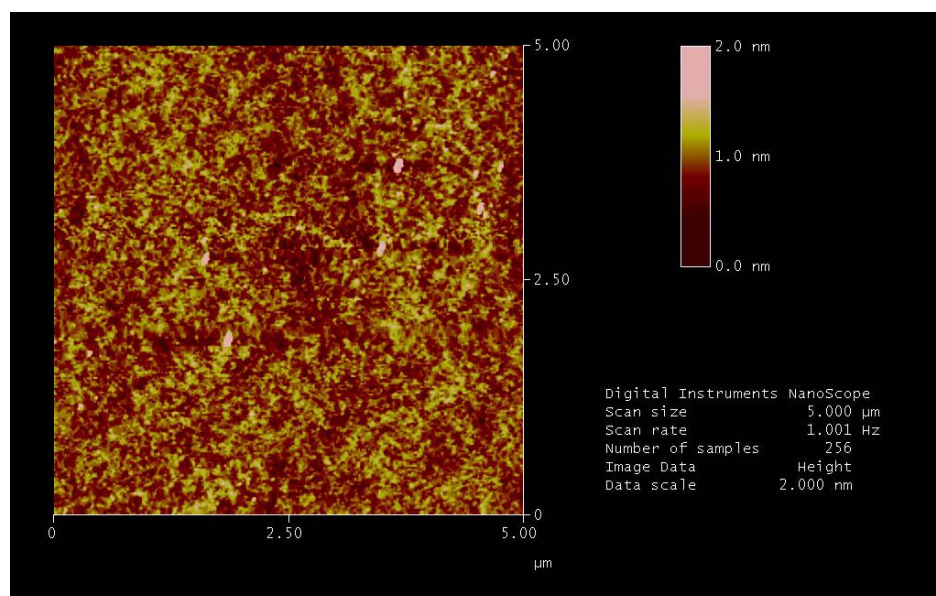

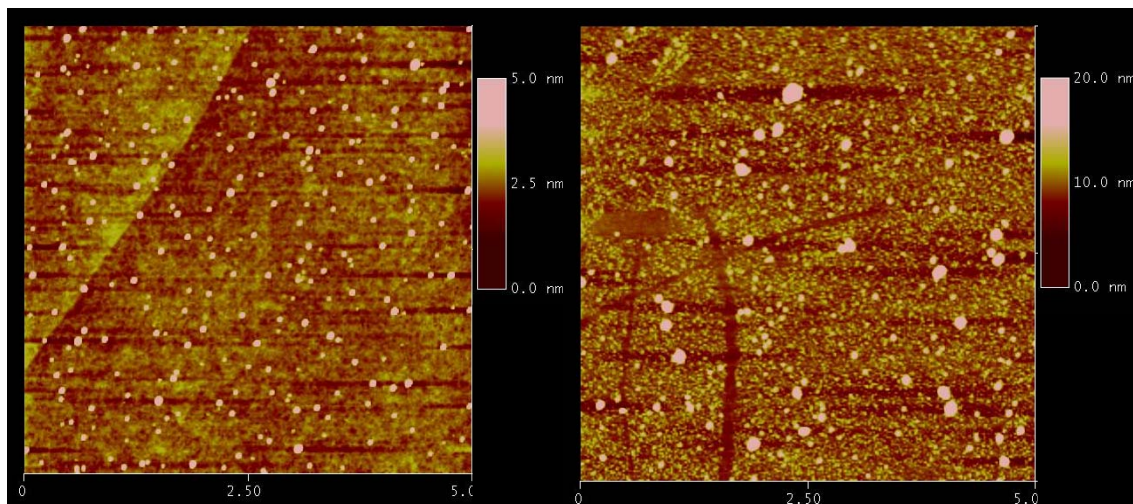**Figure 12. AFM image of a bare silicon wafer.**

Figure 13. AFM images of silicon wafer (left side) and Py11Si SAM (right side) surfaces polymerized for 1 minute.

Nevertheless, at 2 minutes of plasma polymerization (Figure 14) is where the most relevant results have been obtained about the nucleation and growth process. Unmodified silicon wafers polymerized for 1 and 2 min present a very similar topography. In contrast, nuclei on SAM-modified silicon wafer cover practically the entire surface. It can be assumed that the increasing effect of the polymer deposition is caused by the pyrrole-terminated group of the monolayer. The higher affinity of the monomer towards the chemical group of the monolayer seems to lead to a faster deposition on the surface, acting as a nucleation seed for the polymer growth, in the same way that it has been reported for the electrochemistry polymerization. In addition, it should be noted that there are clear signs that nuclei growth suggests the formation of a first PPy layer by nuclei merge.
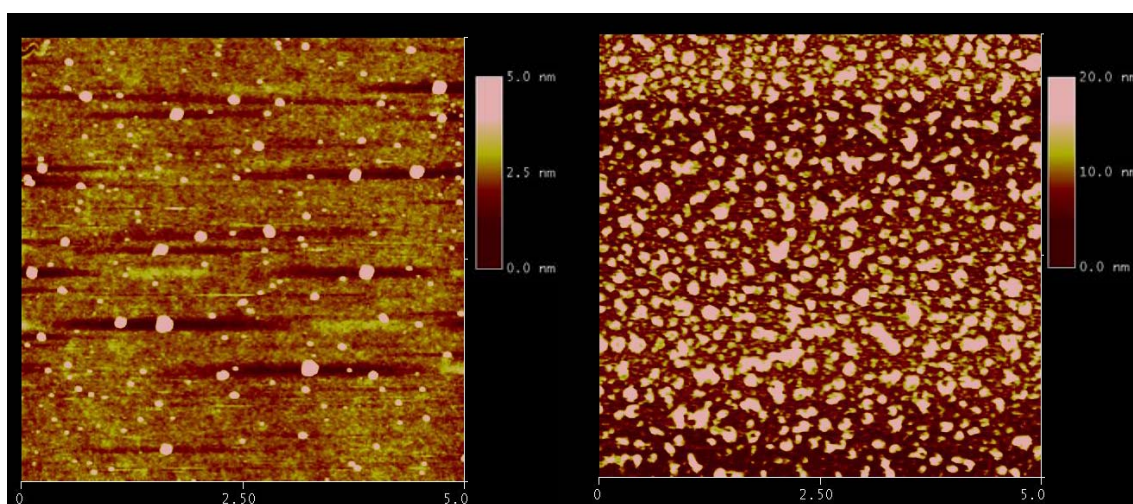

Figure 14. AFM images of silicon wafer (left side) and Py11Si SAM (right side) surfaces polymerized for 2 minutes.

100

After 5 minutes of plasma polymerization on the bare silicon wafer, more nuclei have been deposited in comparison with the previous ones. Besides, related to the topography of the Py11Si SAM polymerized for 5 minutes (see Figure 15), it is more convenient to discuss about polymer growth rather than nucleation. This is due to the nucleation-growth mechanism. Once the nuclei have been deposited and stabilized on the surface, more molecules can be bound and, as a result, there is a growth of the nuclei. This is produced over the entire surface in such a way, that a polymer layer is obtained. The initial stage has been observed in Figure 14, where grain boundaries have merged due to nuclei expansion. Then, the mechanism happens again to obtain a polymerization layer by layer.[22] As a consequence, at 5 min of plasma polymerization on SAM-modified silicon wafer, the nuclei deposition on a PPy thin film can be observed.
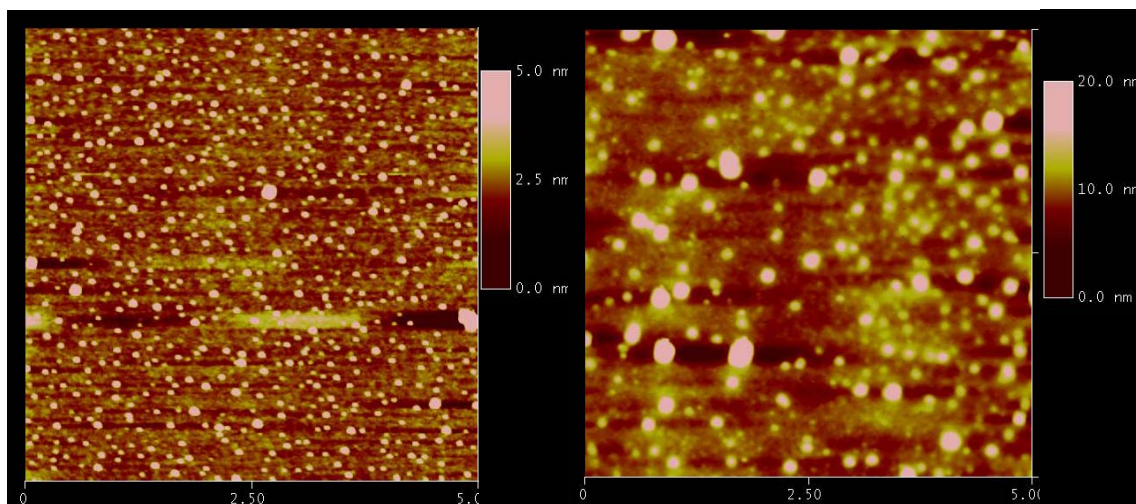

Figure 15. AFM images of silicon wafer (left side) and Py11Si SAM (right side) surfaces polymerized for 5 minutes.

3.4.5.2 TOF-SIMS

After the AFM study, PPy deposition has been characterized by TOF-SIMS in order to measure the amount of PPy deposited onto the surfaces. The aim is to corroborate that SAMs really improves PPy deposition.

A number of studies have been done to characterize PPy by TOF-SIMS. Most of them were focused on negative ion mode, as no relevant structural information was found on cationic PPy chains.[23] No evidence for molecular cations of pyrrole $[M \pm H]^+$ at m/z 66 and 68 were found, therefore no positive TOF-SIMS spectra have been included in this

part. On the other hand, in the negative ion mode has been concluded that the peak at m/z 26 is characteristic of PPy.[24-26] This signal has been assigned to the CN^- anion due to fragmentation of the pyrrole unit, indicating that PPy is unstable under ion bombardment. Furthermore, since the CH_2^- anion was present in the survey spectra and forms part of the pyrrole chemical structure, it could be interpreted as another indicator of PPy chains. Nonetheless, this anion is observed typically in hydrocarbons molecules also, which could affect the posterior analysis.

In all the spectra, the band at m/z = 60, corresponding to the SiO_2^- ion and characteristic of silicon wafer surfaces, is pointed out. Figure 16 presents the TOF-SIMS spectra of the bare silicon wafer and the Py11Si SAM surfaces polymerized for 1 minute. As commented before, the CN^- signal can be seen in both surfaces. In addition, a very intense peak, which had not been discussed previously, can be observed at m/z 42. This fragment is assigned to the CNO^- anion, which was generated from the recombination of oxygen and CN^-. To our knowledge, this peak had not been taken in account until now and evidences from this study suggest that CNO^- ions can be considered as characteristic features of PPy deposition. Additionally, the pyrrole anion, $C_4H_4N^-$ m/z 66, is pointed out too. Usually, it is not very common to find this peak due to polymer fragmentation, but in our spectra it has a relatively high intensity, especially in SAM-modified surfaces. Obviously, it proves the presence of PPy chains and therefore it has been added in the analysis.
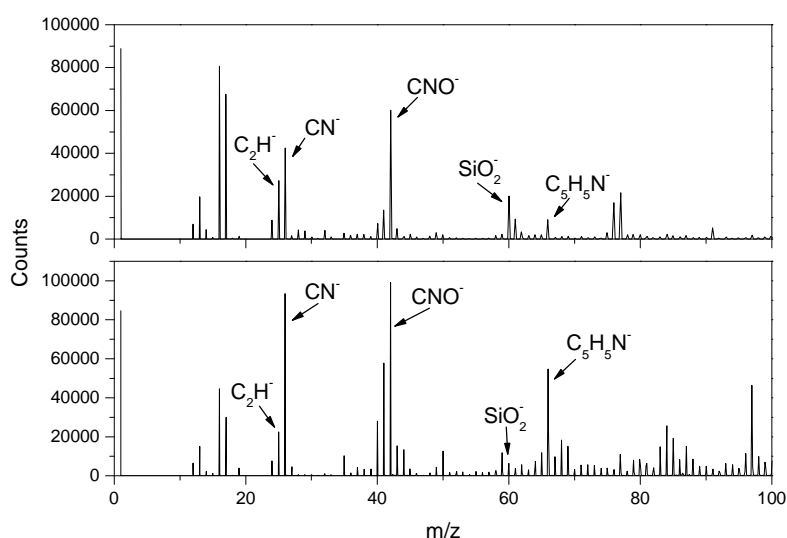

Figure 16. Negative TOF-SIMS spectra of the silicon wafer (upper) and the Py11Si SAM (lower) surfaces polymerized for 1 minute.

Relative intensities normalized with respect to SiO_2^- of the different ions are shown in Table 2. The enormous relative intensities differences between unmodified and SAM-modified surfaces for CN^-, CNO^- and $C_4H_4N^-$ fragments means that more polypyrrole has been deposited on SAM-modified surfaces and corroborates the idea that it is caused by the pyrrole-terminal monolayer. As it was observed in the AFM characterization, SAM-modified silicon wafers present more PPy nuclei onto their surfaces than unmodified. Therefore, it seems normal that the ratio of polypyrrole indicator fragments be higher for Py11Si SAMs. Besides, the variation in the CH_2^- ratio was not so significant, suggesting that this ion is not as important for the polypyrrole identification on the surface.

Table 2. Relative intensities of C_2H^-, CN^-, CNO^- and $C_4H_4N^-$ ions on silicon wafers and Py11Si SAM-modified surfaces polymerized for 1 minute.

Fragment	m/z	Intensity	
		Si	SAM
C_2H^-	25	1.35	3.58
CN^-	26	2.11	14.88
CNO^-	42	2.99	15.82
$C_4H_4N^-$	66	0.45	12.03

Figure 17 provides the negative TOF-SIMS spectra of silicon wafers and Py11Si SAM surfaces polymerized for 2 minutes. The same characteristic fragments were observed and studied. Their relative intensities normalized with respect to SiO_2^- are presented in Table 3. Similar results were obtained for these samples. Surfaces modified with 11-(pyrrol-1-yl-undecyl)dimethylchlorosilane reveal higher ratio values of polypyrrole indicator fragments.
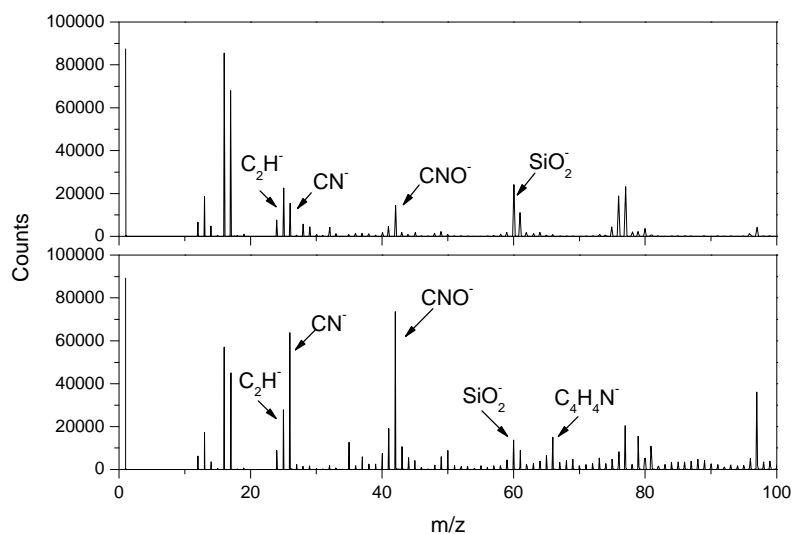
Figure 17. Negative TOF-SIMS spectra of the silicon wafer (upper) and the Py11Si SAM (lower) surfaces polymerized for 2 minutes.

Table 3 provides the relative intensities of PPy fragments indicators on unmodified and SAM-modified silicon wafers polymerized for 2 min. Again, SAM-modified surface shows higher intensities, confirming a major deposition onto it

Table 3. Relative intensities of C_2H^-, CN^-, CNO^- and $C_4H_4N^-$ on the silicon wafer and the Py11Si surfaces polymerized for 2 minutes.

		Intensity	
Fragment	m/z	Si	SAM
C_2H^-	25	0.94	2.02
CN^-	26	0.64	4.63
CON^-	42	0.60	5.34
$C_4H_4N^-$	66	0.03	1.10

AFM has revealed the PPy deposition by observing the surface topography, while TOF-SIMS has confirmed chemically that more PPy has been deposited on SAM-modified surfaces.

3.5 DEPOSITION OF POLYPYRROLE THIN FILMS

3.5.1 EXPERIMENTAL PART

In the above section, adjusting the base and final pressure has enabled to control a slow monomer entrance to observe the PPy nucleation. In the next experiments, some changes in the experimental parameters were done in order to increase the polymer thickness range to work with. The main difference consisted of varying the pyrrole flow rate into the reactor chamber and, thereby, the deposition rate. Since pyrrole has a low vapour pressure and it affects to its introduction into the chamber, a possible solution was to increase the temperature of the Erlenmeyer containing the monomer in order to facilitate the pyrrole evaporation. To carry out the experiments, the temperature was adjusted using a thermocouple and controlled through a temperature controller (Fuji Electric). I

The base pressure reached in the reactor chamber was 0.04 mbar, then, the pyrrole was heated to 50 ºC and the flow was controlled through a needle valve to achieve a final pressure of 0.2 mbar. The plasma power peak was kept at 20 W. Different duty cycles were employed in the polymerizations: 90% (10s ON / 1s OFF) and 50% (5s ON / 5s OFF and 1s ON / 1s OFF). Polymerization times ranged from 1 to 20 minutes.

3.5.2 CHARACTERIZATION OF POLYPYRROLE THIN FILMS

3.5.2.1 Monomer flow rate

To increase the introduction of pyrrole into the reactor chamber, the temperature of the Erlenmeyer containing the monomer was raised to 50ºC and the final pressure was adjusted via needle valves. Nevertheless, the introduction of the monomer to synthesize thin films is generally characterized by the flow rate instead of using the pressure.

The flow rate of a monomer is given by the volume of the gas at standard temperature and pressure (273 K and 1 atm) per unit time (cm^3_{STP}/min, which is often designated as standard cubic centimeters per minute, sccm).

In order to calculate the flow rate some concepts should be taking into consideration. Assuming that gas and vapours for plasma polymerization act as ideal gases, they are ruled by the ideal gas law:

$$PV = nRT \qquad (3)$$

For this equation, V is the reactor chamber volume and it has a fixed volume, R is the ideal gas constant and the temperature T is maintained constant during the polymerization. Then, it is possible to assume that a change in the number of gas molecules in the system, n, is directly proportional to the variation of pressure in a closed volume. Furthermore, because a gaseous system can be defined by the product PV, the volume flow rate F of a gas is given by:

$$F \equiv \frac{d(PV)}{dt} \qquad (4)$$

Thus, the monomer flow rate can be calculated using the next equation:

$$F = \frac{dP}{dt} \times V_{reactor} \qquad (5)$$

Determination of the flow rate was done by the following procedure:
First of all, the reaction chamber was evacuated to the base pressure. Then, the valves connecting the pyrrole and the chamber were opened. The system was left until a steady-state flow of monomer was established (the pressure must coincide with the final pressure of the experimental conditions). Afterwards, the valve that connects the reactor with the pump was closed and the variation of pressure with time was followed. Therefore, the flow rate is given by equation 5, where P is expressed in mbar, t in seconds and V in litres. To express the monomer flow rate in sccm the next conversion was applied:

$$1\frac{mbar \times l}{s} \equiv 5.92 sccm \qquad (6)$$

In addition, a correction must be done in the calculation above. Because the reactor is not a hermetically isolated system, leakages must be taken in account when determining the flow rate. The flow rate measured in the experiment (F_{TOT}) was the

sum of the leakage flow (F_{LEAK}) and the monomer flow (F_{MON}) in fact. Leakages in the reactor, valve connections and Erlenmeyer affect the measured flow. The more leakages in the system, the faster the pressure increases. For that reason, it is necessary to calculate the leakage flow as well.

The leakage flow was estimated in a similar way than the previous experiment.
The reactor chamber was evacuated to the base pressure. Then, an empty Erlenmeyer was connected to the reactor and the valves connecting the Erlenmeyer and the reactor were opened. The system was left until a steady-state pressure was achieved. Afterwards, the valve that connects the reactor with the pump was closed and the variation of pressure with time was followed. The leakage flow was obtained by using equation 5 as well.

Finally, the monomer flow rate was calculated by equation 7:

$$F_{MON} = F_{TOT} - F_{LEAK} \tag{7}$$

It should be emphasized that determination of the flow rate from the pressure rise holds only in gas molecular regime, that is, at pressures below 0.001 mbar. On the other hand, at pressures above 0.1 mbar, it is necessary to change to the viscous flow model and adsorption/desorption gas processes on the walls become important. In this sense, F_{MON} determination is approximate as the F_{DESORP} term has not been included in equation 7.
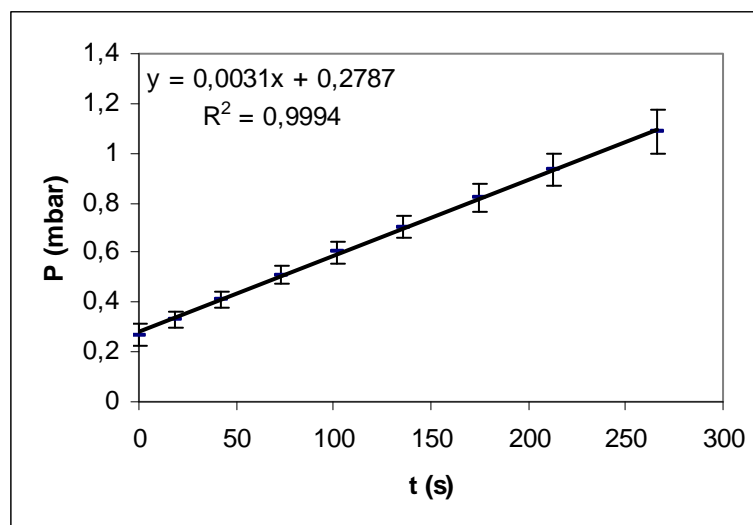

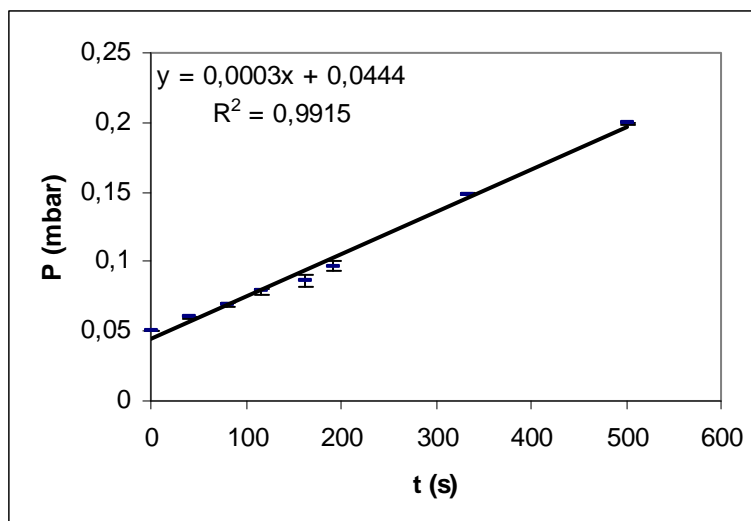**Figure 18. Total flow rate.**

Figure 19. Leakage flow rate.

The product of the slope per the reactor volume gives the flow rate. The slope in Figure 18 is $3.1\cdot10^{-3}$ mbar/s and the reactor volume 80.1 L, then the total flow rate according to Equation 5 and Equation 6 is 1.47 sccm. The slope in Figure 19 is $3\cdot10^{-4}$ mbar/s, and the leakage flow is 0.14 sccm. Therefore, according to Equation 7, the pyrrole flow rate employed in the experiments is 1.33 sccm.

3.5.2.2 Ellipsometry

Another parameter that should be defined in plasma polymerization of thin films is the polymer deposition rate, which is closely correlated with the flow rate of monomer calculated in the above section.

Ellipsometry measures the change in the polarization state of light when it reflects in the sample. Due to this change, this technique is commonly used to characterize thickness and optical constants of materials. Next, the thickness results obtained for the PPy deposition on silicon wafer and on Py11Si SAM-modified silicon wafer are shown. They have been classified into three categories, depending on the duty cycle employed.
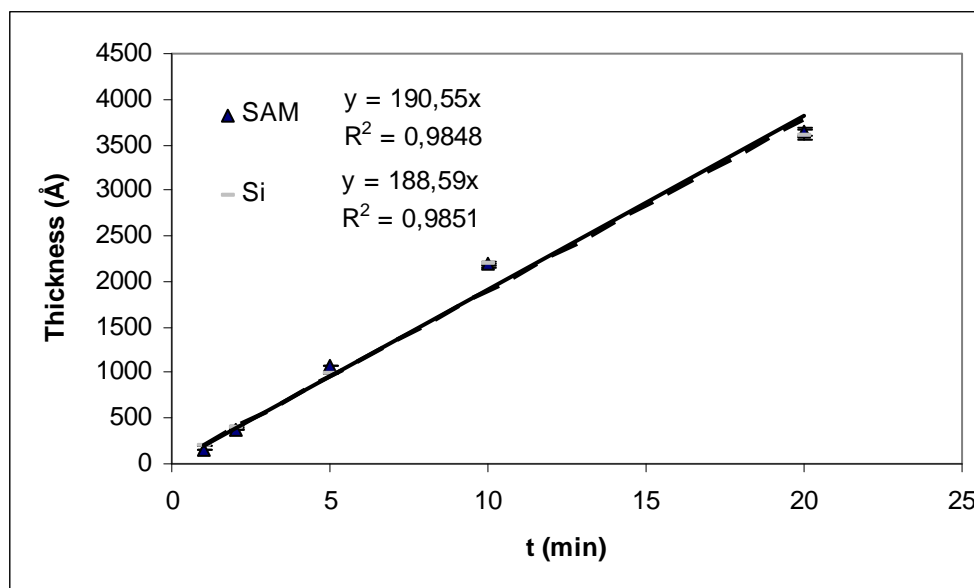
- *90% duty cycle (10s ON / 1s OFF)*

Figure 20. Film deposition rate for plasma polymerization of pyrrole at 20 W with a 90% duty cycle (10s ON / 1s OFF).

The deposition rate for plasma polymerized pyrrole at 20 W plasma power with a 90% duty cycle is 18.9 nm/min for unmodified silicon wafer substrates and 19.1 nm/min for SAM-modified silicon wafer substrates.

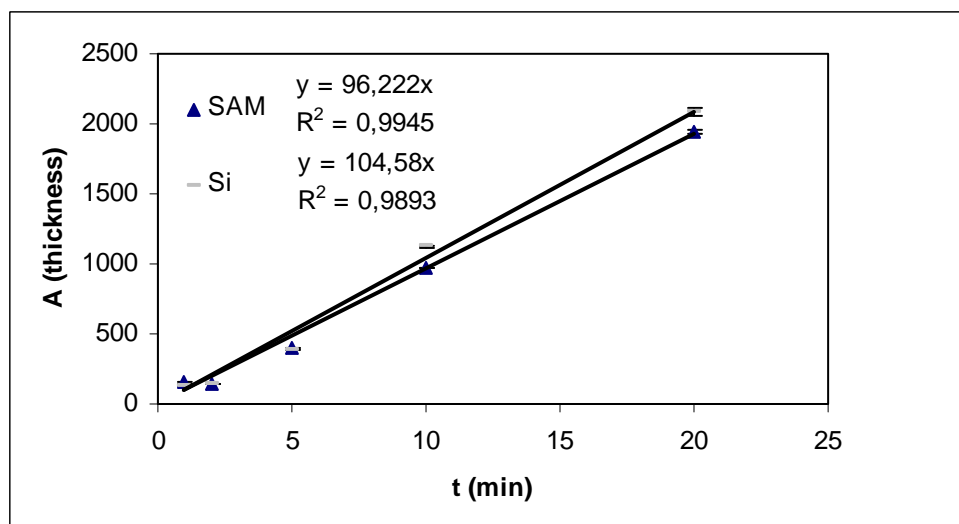- *50% duty cycle (5s ON / 5 s OFF)*

Figure 21. Film deposition rate for plasma polymerization of pyrrole at 20 W with a 50% duty cycle (5s ON / 5s OFF).

The deposition rate for plasma polymerized pyrrole at 20 W plasma power with a 50% duty cycle (5s ON / 5s OFF) is 10.4 nm/min for unmodified silicon wafer substrates and 9.6 nm/min for SAM-modified silicon wafer substrates.
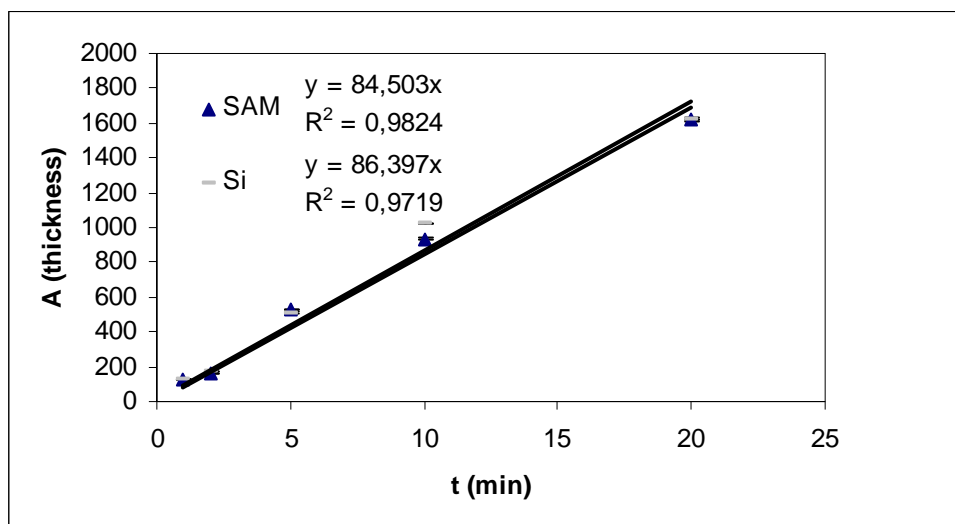
- *50% duty cycle (1s ON / 1s OFF)*

Figure 22. Film deposition rate for plasma polymerization of pyrrole at 20 W with a 50% duty cycle (1s ON / 1s OFF).

The deposition rate for plasma polymerized pyrrole at 20 W plasma power with a 50% duty cycle (1s ON / 1s OFF) is 8.6 nm/min for unmodified silicon wafer substrates and 8.5 nm/min for SAM-modified silicon wafer substrates.

To sum up, the deposition rates for plasma polymerized PPy thin films with different duty cycles on SAM-modified and non-modified silicon wafers are displayed in Table 4.

Table 4. Deposition rates (nm/min) for plasma polymerized PPy thin films with different duty cycles on SAM-modifies (SAM) and non-modifies (Si) silicon wafers.

	Duty cycle		
	90% (10s / 1s)	50% (5s / 5s)	50% (1s / 1s)
Si	18.9	10.4	8.6
SAM	19.1	9.6	8.5

The first remarkable finding is that there is no difference between SAM-modified and non-modified samples. The deposition rate for each one of the three experiments can be practically considered the same. Thus, it seems that pyrrole-terminated monolayers neither influences nor has any enhancing effect on the PPy deposition rate. Since the amount of pyrrole introduced in the plasma reactor is higher in comparison with section

3.3.4, it is not possible to observe the nucleation enhancing effect that causes the monolayer in the deposition process.

Turning now to the duty cycle, the highest deposition rate corresponds to the 90% duty cycle, ~19 nm/min; the second one is the 50% (5s ON / 5s OFF), ~10 nm/min, and the lowest deposition rate corresponds to the 50% (1s ON / 1s OFF), ~8.5 nm/min. Polymerization with a 90% duty cycle has during longer time the plasma on and it causes the activation of more pyrrole species, therefore, there are more chances of PPy to be deposited on the surface. It seems logical that generating a major number of pyrrole radicals the deposition rate increases, because the polymerization pathways increase as well.

Besides, the two set of experiments performed with a 50% duty cycle present a small variation of the sample thickness. Despite having the plasma on the same time during the polymerization process, the deposition rate is slightly different. Samples in which the plasma was on for longer time (5 seconds) during the cycle present a higher deposition rate than films deposited with a shorter on time (1 second). The observed increase could be attributed to a major effectiveness in the reactive species generation. During these 5 seconds, more reactive species can be created in comparison with the total species created during 1 second five times. Thereby, more reactive species generated entails a higher deposition rate.

3.5.2.3 FT-IR

FT-IR measurements were performed in order to study the functionality of polypyrrole. One of the drawbacks of using plasma conditions is the loss of the monomer functionality. Applying a high-wattage can lead to an unexpected chemical structure and composition due to monomer fragmentation or unwanted reactions in the glow discharge. For instance, opening of the aromatic chain and monomer oxidation, or even polymer backbone oxidation, are some of the effects that can happen during PPy plasma polymerization. Generally, working in a low-wattage mode and controlling the duty cycle parameter are the most common recommendations to avoid these unwanted polymer modifications.

In these experiments, the input power was kept constant at 20 W and the duty cycle varied in order to study the retention of the functionality, and to choose the

experimental conditions which lead to the most chemically uniform structure and composition of PPy films.

As it was commented before, the glow discharge can result in the formation of new functionalities that in chemical or electrochemically synthesised PPy films are not so evident. The main absorbance bands for plasma polymerized PPy thin films found in literature[27-29] are depicted next:

- 3380 cm^{-1} stretching vibration of aromatic amines, -NH.
- 2880 - 2960 cm^{-1} symmetric and asymmetric C-H stretching
- 2200 cm^{-1} stretching vibration of nitriles, -C≡N.
- 1550 - 1650 cm^{-1} in-plane vibrations of C=C and C=N and N-H vibration.
- 1400 - 1440 cm^{-1} stretching vibration of C=C and N-H bending.

All the spectra exhibit a broad band between 3200 cm^{-1} and 3500 cm^{-1}, which is due to N-H stretching vibration of primary and secondary amines and imines. In our experiments, the 3380 cm^{-1} peak has been assigned to the aromatic amine in the pyrrole group. Several intense bands slightly below 3000 cm^{-1} can be observed, which has been assigned to the C-H stretching vibration of saturated hydrocarbons: the 2885 cm^{-1} peak represents the sp^3 –CH$_3$ symmetric band, the 2920 cm^{-1} is associated with the sp^3 –CH$_2$– asymmetric vibrations and the 2955 cm^{-1} the sp^3 –CH$_3$ asymmetric vibrations. The 2200 cm^{-1} band, assigned to the nitrile group, is due to the ring-opening of the pyrrole monomer, as a consequence, it should be a characteristic peak for plasma polymerized PPy films. Then, peaks at 1620 and 1400 cm^{-1} are a superposition of unsolved bands determined by the C=C, C=N and N-H bonds.

Figure 23 shows the FT-IR spectra of plasma polymerized films with a 90% duty cycle obtained after 1, 5 and 20 minutes of polymerization. In samples polymerized for 1 and 5 minutes (green and red lines), the absorbance bands intensity is barely significant. On the other hand, both samples polymerized for 20 minutes (blue and pink line) show very intense bands. These bands coincide with the characteristic features of PPy films remarked before. FT-IR is a surface characterization technique, but for very thin samples, like the ones obtained for 1 and 5 minutes of polymerization, it is difficult to work accurately as no intense bands are observed. Similar results have been found studying the spectra obtained with different duty cycles. The spectra of these experiments can be found in annexes. Because of that, samples polymerized for 20 minutes seem thicker enough to deal with.
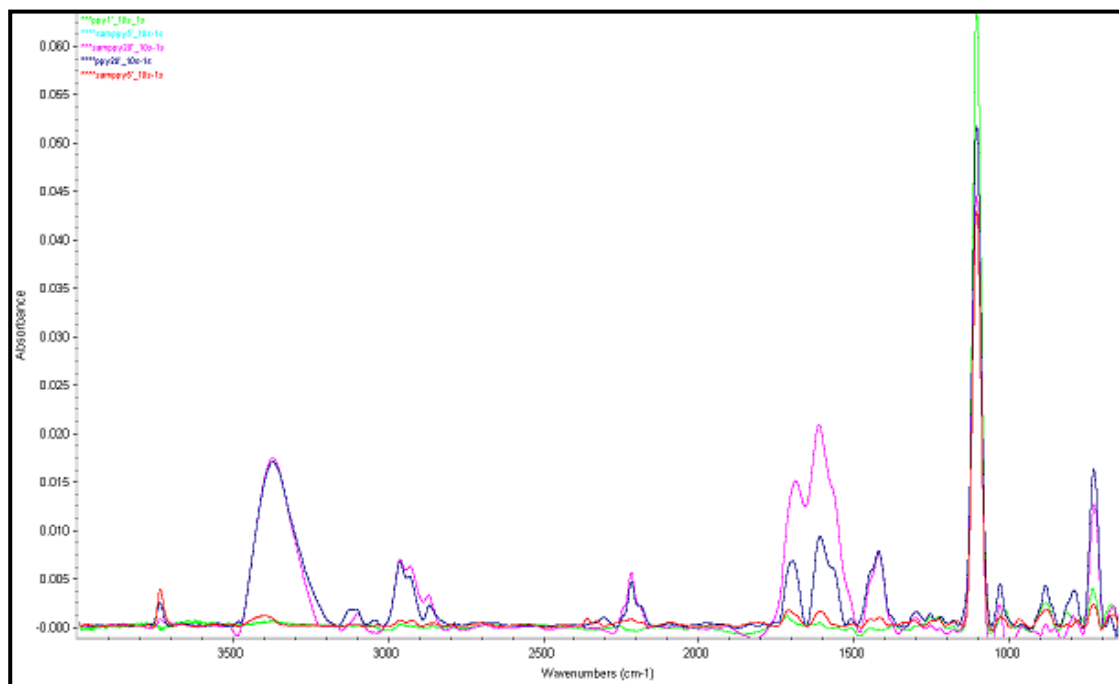
112

Figure 23. FT-IR spectra of plasma synthesized PPy films with a 90% duty cycle at different polymerization times: 1 min green line, 5 min red line and 20 min pink (silicon wafer) and blue (SAM-modified silicon wafer) lines.
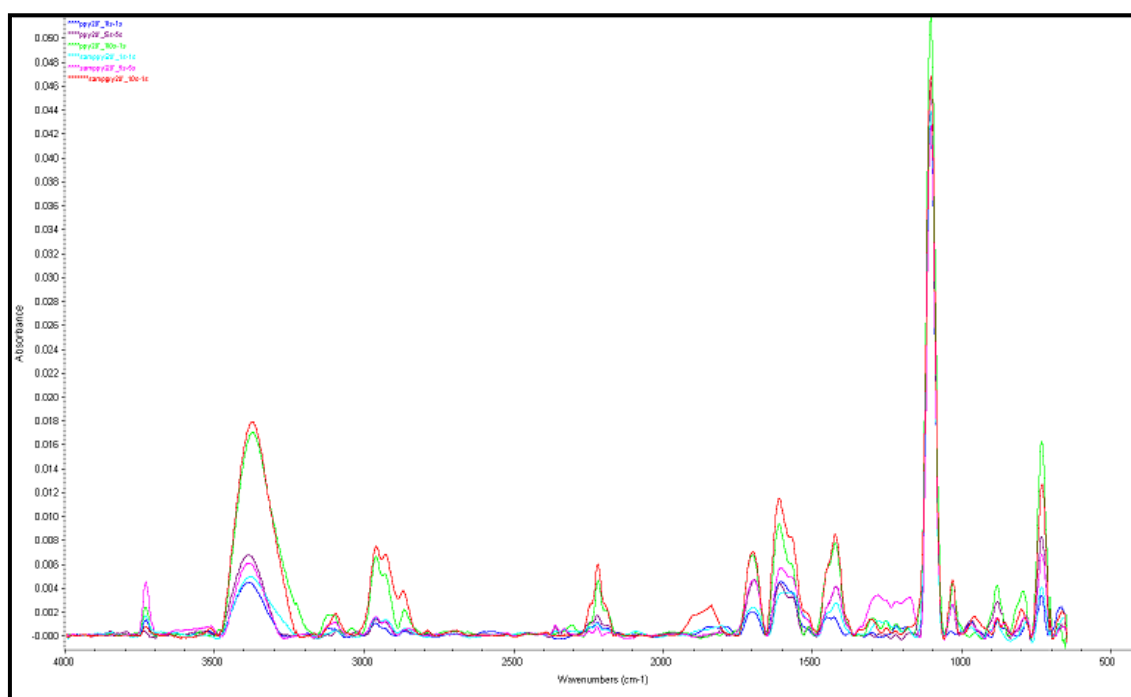

Figure 24. FT-IR spectra of plasma polymerized PPy films deposited after 20 min with different duty cycles: 90% (10s ON / 1s OFF) green (silicon wafer) and red (SAM-modified silicon wafer) lines, 50% (5s ON / 5s OFF) violet (silicon wafer) and pink (SAM-modified silicon wafer) lines and 50% (1s ON / 1s OFF) blue (silicon wafer) and cyan (SAM-modified silicon wafer) lines.

The FT-IR spectra of plasma polymerized PPy films deposited after 20 minutes can be observed in Figure 24. The purpose is trying to study and differentiate the chemical

structure of PPy thin films according to their duty cycle. The most intense bands are observed for the 90% duty cycle, then the 50% (5s ON / 5s OFF) duty cycle and, at last, the other 50% (1s ON/ 1s OFF) duty cycle. These results agree with the ones obtained by ellipsometry according to thickness. As it was expected, the thicker the film is, the more intense the absorbance bands are.

One of the most intense bands is situated at 3380 cm^{-1}, which correspond to aromatic amines. Therefore this signal corroborates the presence of the aromatic structure of PPy on the surface and what is more important, it demonstrates that a large quantity of the polymer backbone has not suffer from aromatic opening, as it was expected. The presence of this signal indicates that, mainly, the polymerization has been carried out by the pyrrole activation and the posterior bond formation among them to form a cross-linked polymer. On the other hand, the absorbance band at 2200 cm^{-1} corroborates a loss of the PPy functionality as well. This band correspond to a nitrile group (-CN), which can only be due to the pyrrole group opening. Due to ion or electron bombardment, the energy transference to the pyrrole has been high enough to break the bond between the nitrogen and one of the carbons neighbour. Therefore, the appearance of the nitrile band in plasma polymerization is thought to be caused by the breaking of the molecule. This signal is assumed to be present always in PPy plasma polymerization, as well as aromatic amine indicates the retention of functionality, the nitrile group means a loss of it. Nonetheless, according to literature found for FT-IR spectra of PPy plasma polymerized films,[27,29,30] the aromatic amine band seems much stronger in our samples, showing higher retention of the pyrrole functionality.

To demonstrate this behaviour, Table 5 shows the intensity ratio between the aromatic amine and the nitrile absorbance bands at the different duty cycles studied. The surfaces used for the deposition were a silicon wafer and a Py11Si SAM-modified silicon wafer. As commented above, higher ratios indicate the preservation of the aromatic structure in plasma polymerized films.

Table 5. Intensity ratio between –NH and –CN characteristic absorbance bands for PPy plasma polymerized films deposited on silicon wafer and SAM-modified silicon wafer.

	Duty cycle		
	1s/1s	5s/5s	10s/1s
Si	8.6	8.4	10.8
SAM	20.7	17.7	8.5

Samples modified by self-assembly decrease their intensity ratio, as long as t_{ON} in the duty cycle increases. This seems quite logical because longer t_{ON} lead to ring opening. The lowest ratio value found correspond to the 90% duty cycle, in which the plasma is on for 10 seconds in every cycle. In the other two samples, the difference between them is quite low as the duty cycle is the same. Surprisingly, on bare silicon wafer samples the ratio is practically the same in all the duty cycles. Even it was a little bit higher for the 90% duty cycle, which was thought to be the most affected by the plasma effect. In general, no clear differences were observed among them.

Another point of interest is that SAM-modified intensity ratio value doubles in comparison with unmodified for both 50% duty cycles, suggesting that SAM-modified surfaces show higher retention of functionality. It seems that the monolayer promotes PPy deposition with a better ring retention. However, these results need to be interpreted with caution as this finding is not transferable to the 90% duty cycle. In this duty cycle, bare silicon wafer samples have a higher intensity ratio in comparison with the SAM-modified. Thus, it is likely that using t_{ON} and t_{OFF} about seconds do not importantly influence on the polymer structure and its effect could be only decrease of the deposition rate, as pointed out in section 3.5.2.2.

3.5.2.4 XPS

XPS measurements were carried out on bare copper substrate, Py6SH, Py6SeH, Py12SH and Py12SeH SAM-modified copper polymerized for 1 minute. Spectra of copper and Py12SH SAM-modified copper polymerized for 1 minute are presented in Figure 25 and Figure 26 respectively. The corresponding spectra for polymerization on Py6SH, Py6SeH and Py12SeH SAMs can be found in annexes as they show very similar results. XPS is a surface technique, which maximum depth analysis is ~10 nm and the PPy coating deposited on the substrates is ~20 nm thick. Therefore, the XPS signals are attributed to the polymer as no traces of copper substrate have been detected. No sign of Cu is the proof of continuous coverage by PPy film of copper substrate. Actually, only three peaks have been found in all the spectra: at 285 eV appears the C 1s signal, at 400 eV the N 1s and at 530 eV the O 1s. The most intense signals are assigned to carbon and nitrogen atoms which form the PPy backbone. Additionally, the appearance of the oxygen peak can be due to atmospheric contaminants and oxidized species created during the plasma process.
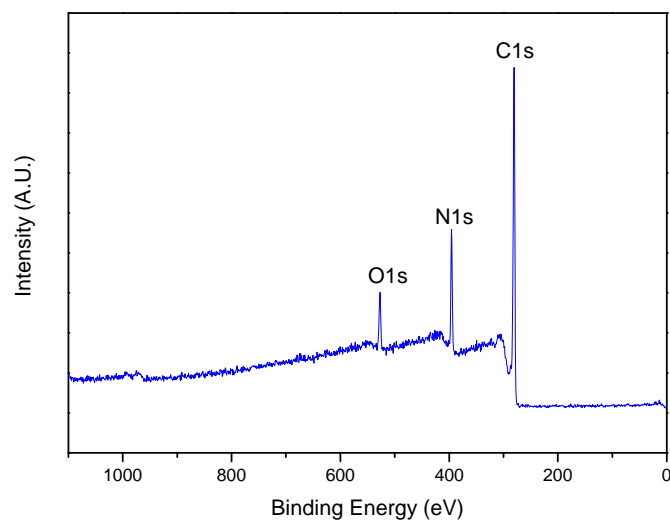
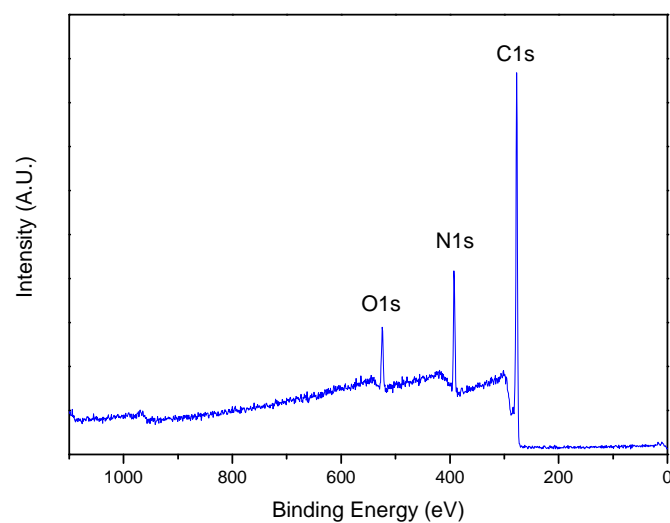**Figure 25. XPS spectrum of a copper substrate polymerized for 1 min.**

Figure 26. XPS spectrum of a Py12SH SAM-modified copper substrate polymerized for 1 min.

Table 6 shows the chemical composition of the different samples obtained by XPS analysis, which includes the percentage of carbon, nitrogen and oxygen. Moreover, Table 7 provides the C/N and C/O ratio values for these samples. The C/N ratio can give an idea about the preservation of the polymer backbone.[31] For a linear, non-defect polypyrrole chain the ratio between carbon and nitrogen should be 4 to 1. Approximately, the plasma polymerized PPy has a ratio of 5 to 1, which is quite close to the ideal value. This is in good agreement with FT-IR results, which assured high

functionality retention in the polymerization process. Additionally, the C/O ratio is related to the pyrrole deposition on the surface and the values obtained present higher quality than films reported by Sahin.[32]

Table 6. XPS surface composition (%) of copper, Py6SH, Py6SeH, Py12SH and Py12SeH SAMs plasma polymerized for 1 min.

	PPy 1 min				
	Cu	Py6SH	Py6SeH	Py12SH	Py12SeH
C 1s	78.2	78.6	79.3	78.4	75.6
N 1s	16.2	14,8	14.7	15.3	11.7
O 1s	5.6	6.6	6.0	6.3	12.7

Table 7. C/N and C/O ratios for the samples polymerized for 1 min.

	PPy 1 min				
	Cu	Py6SH	Py6SeH	Py12SH	Py12SeH
C/N	4.8	5.3	5.4	5.1	6.4
C/O	13.9	12.0	13.4	12.4	5.9

In order to analyze the chemical composition of plasma polymerized films, a more exhaustive study on the carbon and nitrogen signal belonging to the PPy backbone was performed.

XPS deconvolution

The high resolution spectra of these peaks have been fitted using typical bonds studied for PPy and those bonds which can be created because of the plasma discharge.[33-36] As a consequence, the analysis will show the effect of plasma polymerization in the polymer composition and whether the aromatic structure has been preserved or not.

Figure 27 and Figure 28 display the high resolution spectra of N 1s of bare copper and Py12SH SAM-modified copper polymerized for 1 minute (the others high resolution spectra can be found in annexes). The signal has been deconvoluted into three peaks: 399.9 eV (C-N), 398.3 eV (C=N) and 397.6 eV (C≡N). Both C-N and C=N peaks are assigned to typical signals belonging to PPy backbone. On the contrary, the C≡N peak appears as a result of the ring opening.
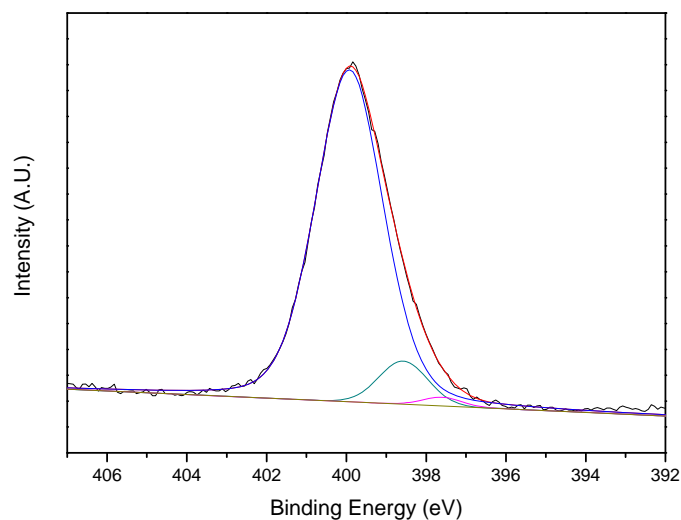
Figure 27. High resolution N 1s XPS spectrum of bare copper polymerized for 1min.

The summary of deconvolution analysis for the N 1s signal can be found in Table 8. Previous investigations of electrochemically synthesized PPy[37] and also of plasma synthesized PPy[33] demonstrated that the peak assigned to the C-N bond is the most intense in the N 1s signal. If there is no opening of the aromatic ring, it seems logical that the C-N peak be the most intense. However, due to the related properties of plasma, the breaking of pyrrole can result in the formation of C=N and C≡N bonds, which means a loss of functionality. Nonetheless, the experimental results agree with literature and confirm the high retention of the polymer functionality as the deconvolution analysis shows again that the most intense peak corresponds to the C-N bond for all the samples. Finally, it should be commented that no differences have been found on the N 1s chemical composition between SAM-modified and not modified samples.
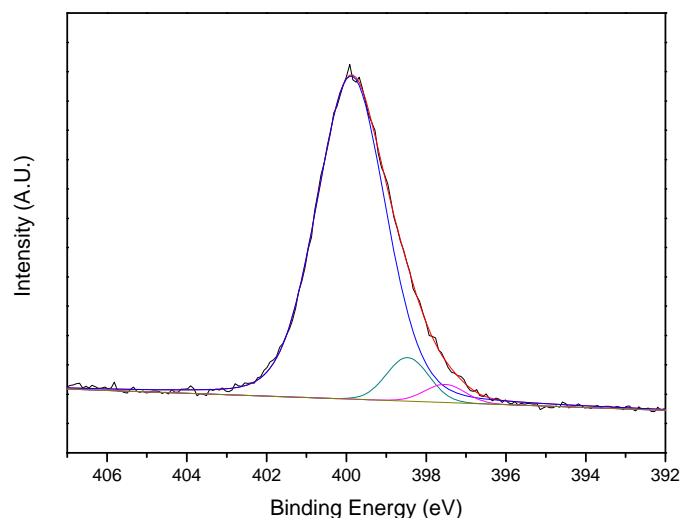
Figure 28. High resolution N 1s XPS spectrum of Py12SH SAM assembled on copper and polymerized for 1min.

Table 8. Chemical composition (%) of the deconvoluted N 1s signal for copper, Py6SH, Py6SeH, Py12SH and Py12SeH SAMs samples polymerized for 1 min.

Bond	Binding Energy (eV)	PPy 1min				
		Cu	Py6SH	Py6SeH	Py12SH	Py12SeH
C-N	399.9	93.6	93.3	94.3	92.0	91.9
C=N	398.5	5.1	5.2	3.6	6.3	5.2
C≡N	397.6	1.3	1.5	2.1	1.7	2.9

The corresponding C 1s high resolution spectra of copper and Py2SH SAM polymerized for 1 min are observed in Figure 29 and Figure 30 (the rest of SAM-modified spectra have been included in annexes). The C 1s signal was deconvoluted employing three peaks: the C-C functionality at binding energy of 284.7 eV, the C-N at 286.0 eV and the C≡N at 288.0 eV. The C-C and the C-N functionalities were used previously in the monolayer characterization. Here, it is necessary to add the C≡N functionality to fit correctly the signal and to give a complete overview of the polymer chemical state, as this peak illustrates the possible breaking of the polymer structure. Furthermore, some bonds of C with oxygen, associated to atmospheric contaminants, can be found in the same energy range. Even though, the percentage of oxygen found on the surface is quite low and can be correlated to a slight oxidation of the copper substrate.
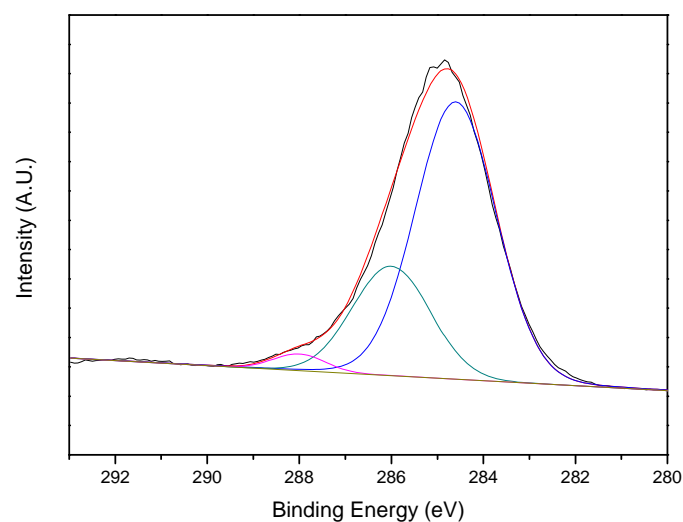
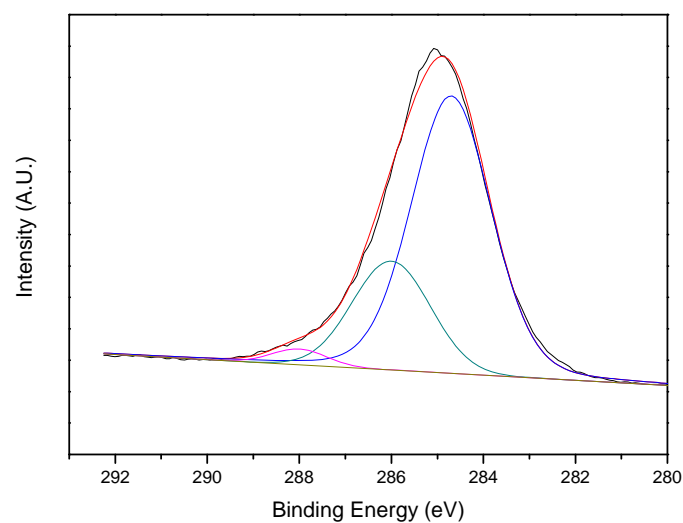**Figure 29. High resolution C 1s XPS spectrum of bare copper polymerized for 1min.**

Figure 30. High resolution C 1s XPS spectrum of Py12SH SAM assembled on copper and polymerized for 1min.

Table 9 summarizes the percentage of the different chemical species assigned to the C 1s signal obtained for all the samples. In general, very similar values were obtained for all them. The most intense peak corresponds to the C-C one, assigned to the three carbon bounds in the pyrrole molecule. Additionally, there is two C-N bond in the pyrrole molecule. Nevertheless, the ratio C-C/C-N is not 3/2 as predicted theoretically. As explained before, in plasma polymerization the pyrrole molecules can be linked randomly. Moreover, the use of plasma results in crosslinked polymers structure, by

which, one pyrrole can be bound to more than one pyrrole. According to the polymerization mechanism in the luminous gas phase discussed in Figure 3, plasma can generate more than one radical in the same activated specie. The formation of these radicals can lead to the chain growth mechanism or to the crosslinking of the polymer by side reaction between chains. Therefore, the C-C/C-N ratio can vary depending on plasma conditions. In addition, some organic contamination and the ring opening effect should be added to the reasons by which the C-C bond peak intensity is so high.

Table 9. Chemical composition (%) of the deconvoluted C 1s signal for copper, Py6SH, Py6SeH, Py12SH and Py12SeH SAMs samples polymerized for 1 min.

		PPy 1min				
Bond	Binding Energy (eV)	Cu	Py6SH	Py6SeH	Py12SH	Py12SeH
C-C	284.7	82.5	83.1	80.8	81.3	86.9
C-N	286.0	14.4	13.9	15.3	15.0	10.9
C≡N	288.0	3.1	3.0	3.9	3.7	2.5

In addition, there has been no evidence of any difference between SAM-modified and non-modified samples in all the XPS results. The surface chemical composition for all the atoms has shown very similar values. This is owed to the fact that the deposition rate is practically the same for both surfaces. Therefore, the SAM-effect can not be appreciated in such conditions and the XPS features are the same on the surface of the plasma polymerized films.

3.5.2.5 Atomic Force Microscopy

The surface topography of plasma polymerized thin films of pyrrole was studied by AFM. In this experiment, the polymerization time was 20 minutes and the substrate employed copper. Figure 31 shows the typical topography for plasma polymerized PPy. Here, the white dots are PPy globules deposit on the film surface. This kind of structure reminds the AFM topography images of samples SAM-modified and polymerized for 5 minutes in section 3.3. In those images, it was discussed that a PPy thin film had been achieved enhanced by the nucleation effect of the monolayer. In addition, that film present the same peak features than the film discussed in Figure 31, according to PPy deposition.
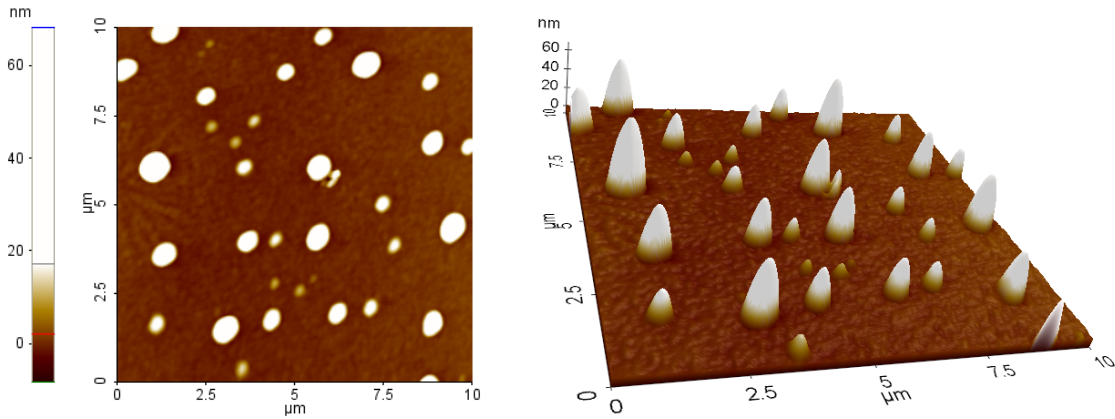
Figure 31. 2D (left side) and 3D (right side) AFM topography images of a PPy thin film plasma polymerized for 20 min on copper.

The globules deposited on the PPy film are placed regularly due to the homogeneous coverage by PPy film of copper substrate. The PPy cluster size are analysed by using the line profile option, which can be seen in Figure 32. The estimated height for peaks found on the surface ranges, approximately, from 50 to 70 nm.
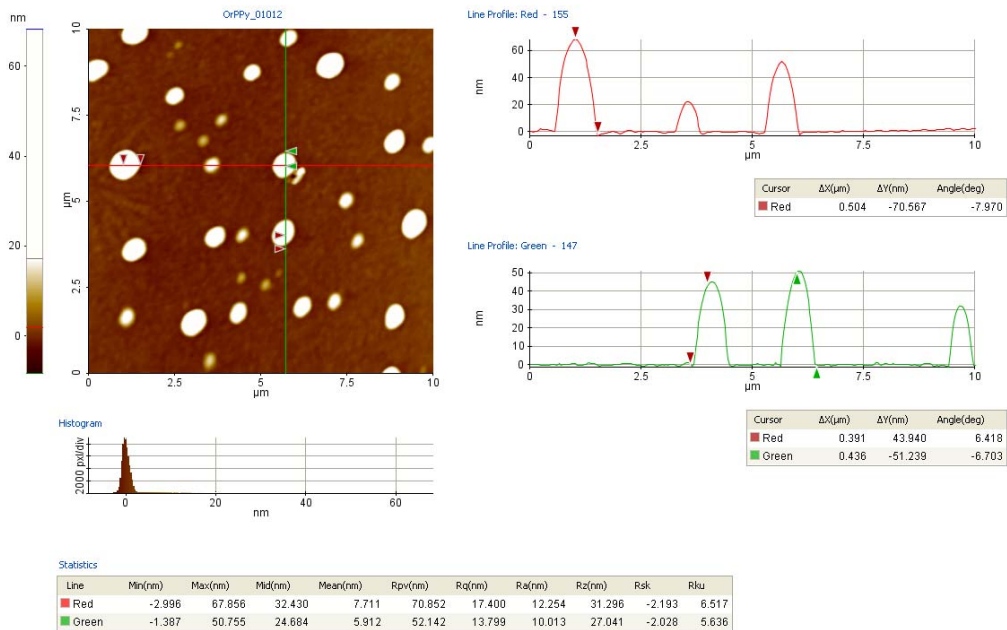

Figure 32. Line profile of an AFM image of PPy thin films plasma polymerized for 20 min on copper.

3.5.2.6 Adhesion test

When a coating is applied to a surface, it is supposed to fulfil the function for which it has been designed. Therefore, it must be adhered for the expected service life. For that purpose, it is necessary a method to evaluate the adhesion between the substrate and the coating. In this case, the adhesion test must cover a procedure to assess the adhesion of coating films to metallic substrates. The test consists in applying and removing a pressure-sensitive tape over cuts made in the film (see more details in section 3.2). Finally, the samples were analyzed by SEM and compared with the appropriate standards shown in Figure 33.
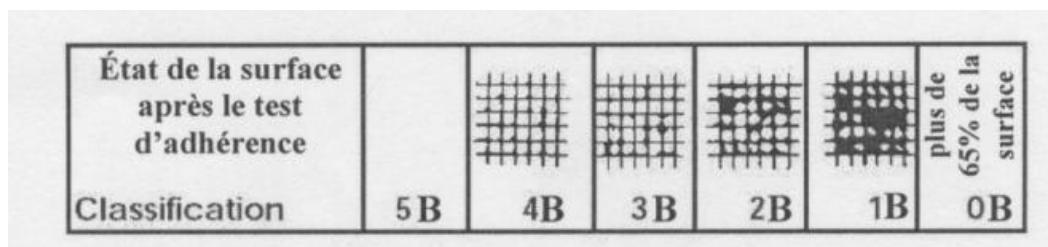

Figure 33. Surface classification after adhesion test.

The adhesion grade was evaluated in accordance with the following scale:

- 5B The edges of the cut are completely smooth and none of the squares of the lattice is detached.
- 4B Small flakes of the coating are detached at intersections; less than 5% of the area is affected.
- 3B Small flakes of the coating are detached along edges and at intersections of cuts. The area affected is 5 to 15% of the lattice.
- 2B The coating has flaked along the edges and on parts of the square. The area affected is 15 to 35% of the lattice.
- 1B The coating has flaked along the edges of cuts in large ribbons and whole squares have detached. The area affected id 35 to 65% of the lattice.
- 0B Flaking and detachment worse than grade 1B.

SEM images

Figure 34 presents the SEM images after performing the adhesion test on the different substrates. Very similar results were obtained for the three samples. No peeling off was observed in the edge of the cuts neither in the bare copper, nor in the SAM-modified copper. According to the ASTM classification, samples present the maximum adhesion possible. One of the advantages of using plasma polymerization, in comparison with other conventional techniques, is the increasing adhesion between polymer and substrate. The activation process of the monomer consists in producing some cations, anions and radical. Besides, by the same process, some radicals are formed on the surface. These radicals, due to its instability are highly reactive. Therefore, radicals on the substrate and from the monomer can react to yield a covalent bond, which increases the polymer adhesion. Because of this, the adhesion test shows the same properties for unmodified and SAM-modified surfaces, just after the polymerization.
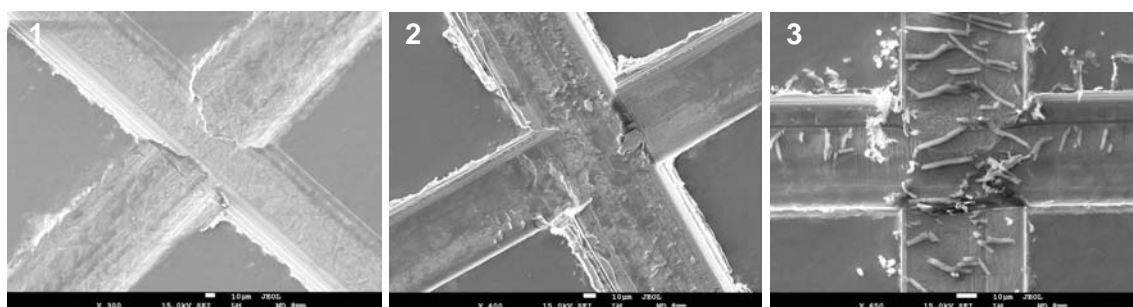

Figure 34. SEM images of adhesion test on PPy films deposited on bare copper (1), Py12SH SAM (2) and on Py12SeH SAM (3).

Nevertheless, as these materials are supposed to be part of some kind of device, the adhesion properties needs to be maintained during the service life of the device. Thus, the same experiment was carried out using three samples which had been polymerized three months ago. The SEM images are presented in Figure 35. Images 22-2 and 22-3, corresponding to Py12SH and Py12SeH polymerized for 2 minutes, present completely smooth cuts and no polymer detachment is observed along the edge. The same as reported in Figure 34, the adhesion grade compared with the standards is the maximum. By contrast, unmodified copper polymerized for two minutes (image 22-1), presents some defects near of the cuts (pointed out by white arrows) attributed to parts of the polymer which have been peeled off.
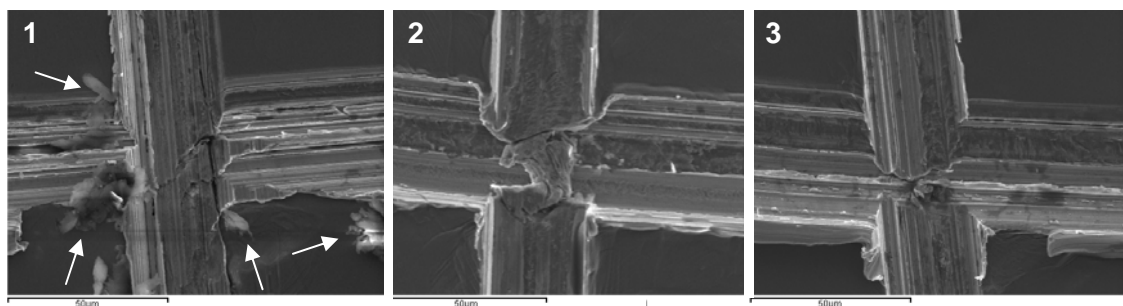
Figure 35. SEM images of adhesion test on PPy films deposited on bare copper (1), Py12SH SAM (2) and on Py12SeH SAM (3) after three months.

In Figure 36 a larger area of the copper sample is observed. In the edge of the cuts can be seen how parts of the polymer has been removed by the tape (white arrows). According to the ASTM classification, this sample presents a 4B adhesion, as approximately less than the 5% of the total surface has been removed.
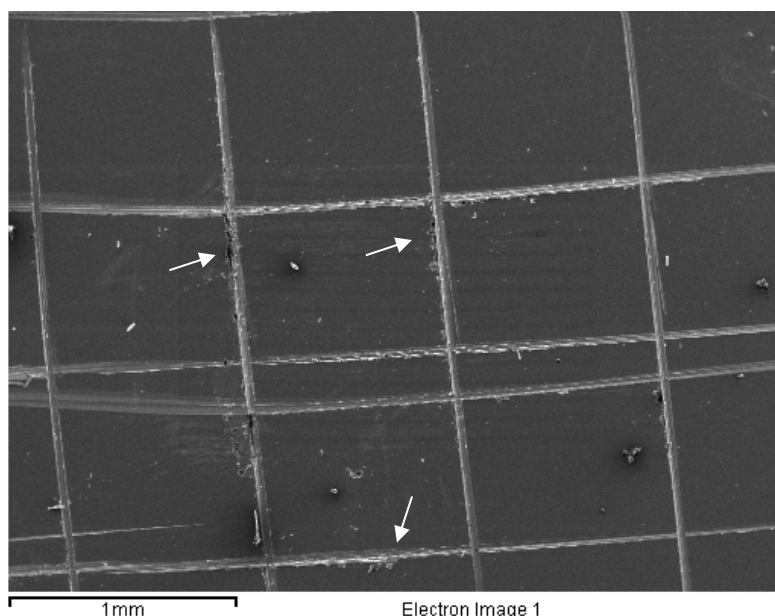

Figure 36. SEM image of the copper surface polymerized for two minutes.

3.6 DOPING PROCESS OF POLYPYRROLE THIN FILMS

3.6.1 INTRODUCTION

In the past, polymers had been considered as insulators or semiconducting materials, depending on their intrinsic band gap. It was not until 1977 when Shirakawa, Heeger and McDiarmid published the article "Synthesis of electrically conducting organic polymers: Halogen derivatives of polyacetylene $(CH)_n$"[38] that caused a breakthrough in the field of polymer synthesis.

All began in 1974 when Shirakawa was performing an acetylene polymerization by Ziegler-Natta catalyst system and he accidentally introduced one thousand times more amount of the catalyst, $Ti(O\text{-}n\text{-}But)_4$. Then, instead of a dark polyacetylene dust he obtained a beautiful silvery film. After that, Shirakawa get through with McDiarmid and Heeger, who were experimenting with a metallic-looking film of the inorganic polymer sulphur nitride, $(SN)_x$. Shirakawa was invited to the University of Pennsylvania in Philadelphia where they continued investigating the modification of polyacetylene films by oxidation with iodine vapour. After measuring the conductivity of the iodine doped trans-polyacetylene, they realised that conductivity has increased ten million times. This was the beginning of conducting polymers or, as they are known as well, synthetic metals. For this discovery, they received the Nobel Prize in Chemistry 2000.

A great number of polymers, such as polyanyline, polythiophene and polypyrrole, have been investigated since that due to their electronic properties and their new wide range of applications. All of these polymers present conjugated double bonds, which consist of alternating single and double bonds. This is the first condition that possesses conducting polymers. The double bond is formed by a σ bond and a π bond. The electrons in the σ bond are localized and they form a covalent bond among carbon atoms. Nonetheless, electrons in the π bond are not so fixed. These electrons are placed in the π orbital and they are perpendicular to the σ bond. The π orbitals in a conjugated system are overlapped and it allows a delocalization of these electrons. However, to become electronically conductor, these polymers need a doping process. The doping process consists of an oxidation or reduction reaction by which an electron is removed or inserted. At that time, when an electric field is applied, the π electrons can move along the molecule chain.

The explanation for this phenomenon is based on the band theory. The electronic properties of a material are determined by its electronic structure. According to the Pauli Exclusion Principle, electrons tend to occupy their corresponding atomic orbital. In a metal, the atomic orbital of an atom overlap with the one of the neighbour atom to form molecular orbitals. Additionally, because there are a huge number of molecular orbitals for an energy level, it is said that they form a continuous band. Then, the highest occupied band for electrons is called valence band and the lowest unoccupied band, the conduction band. The difference between these two bands is the band gap and depending on the band gap the material become conductor, semiconductor or insulator. In a conductor, the valence band and the conduction band are merged, so there is no band gap. Because of this, when an electric field is applied electrons can jump among the different orbitals and they can flow. Contrarily, semiconductors and insulators have a band gap. If it is higher than 3 eV it is considered as an insulator and if it is lower, a semiconductor.
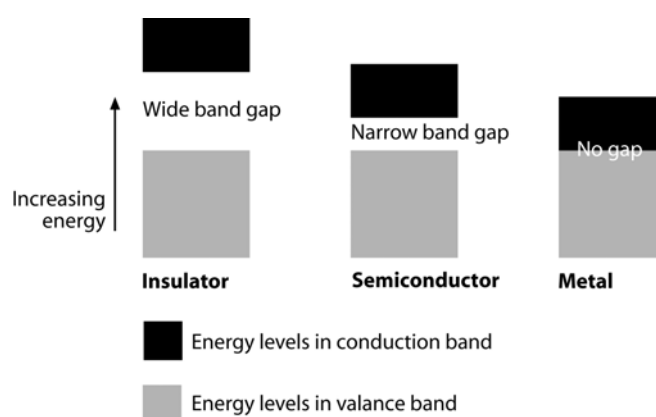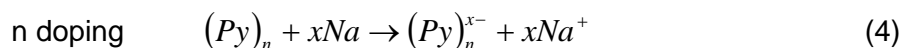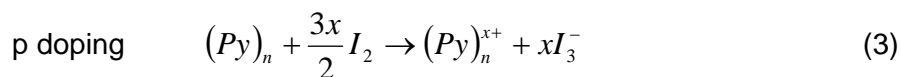

Figure 37. Schematic band gap representation for an insulator, a semiconductor and a metal.

Due to its electronic structure polymers are classified as insulators or semiconductors. However, when the polymer is doped it reaches a bipolaron state, which entails charge formation into the polymer backbone. Due to the formation of these charges, two additional bands are formed between the valence and the conduction band. These new bands can enhance the charge transport because of proximity with the valence and conduction band or, even, they can merge with them, depending on the doping level. As a result, a conducting material is obtained.

As mentioned earlier, the doping process is achieved by an oxidation (p doping) or a reduction (n doping) reaction. The oxidation can be carried out by a halogen and the reduction by an alkali. In the case of polypyrrole, the reactions are:

$$\text{p doping} \qquad (Py)_n + \frac{3x}{2}I_2 \rightarrow (Py)_n^{x+} + xI_3^- \qquad (3)$$

$$\text{n doping} \qquad (Py)_n + xNa \rightarrow (Py)_n^{x-} + xNa^+ \qquad (4)$$

In our experiments, PPy was doped by oxidation (p-doping) using as dopant agent iodine. When an iodine atom approaches to the PPy chain, it subtracts an electron from a π orbital. The iodine becomes an iodide anion (I_3^-) and a positive charge and a radical are generated in the polymer chain. This structure is known as polaron. Afterwards, the same process is repeated. Another iodine atom approaches to the PPy chain and it subtracts another electron and a positive charge and a radical are generated again. The two radicals condense in a new π bond, leaving two positive charges in the PPy chain. This structure is called bipolaron and it is repeated each four pyrrole units along the polypyrrole chain. The bipolaron is the responsible for the electronic movement along the polymeric chain. Additionally, to maintain the electroneutrality principle, the iodide anions are placed next to the chain by electrostatic attraction.
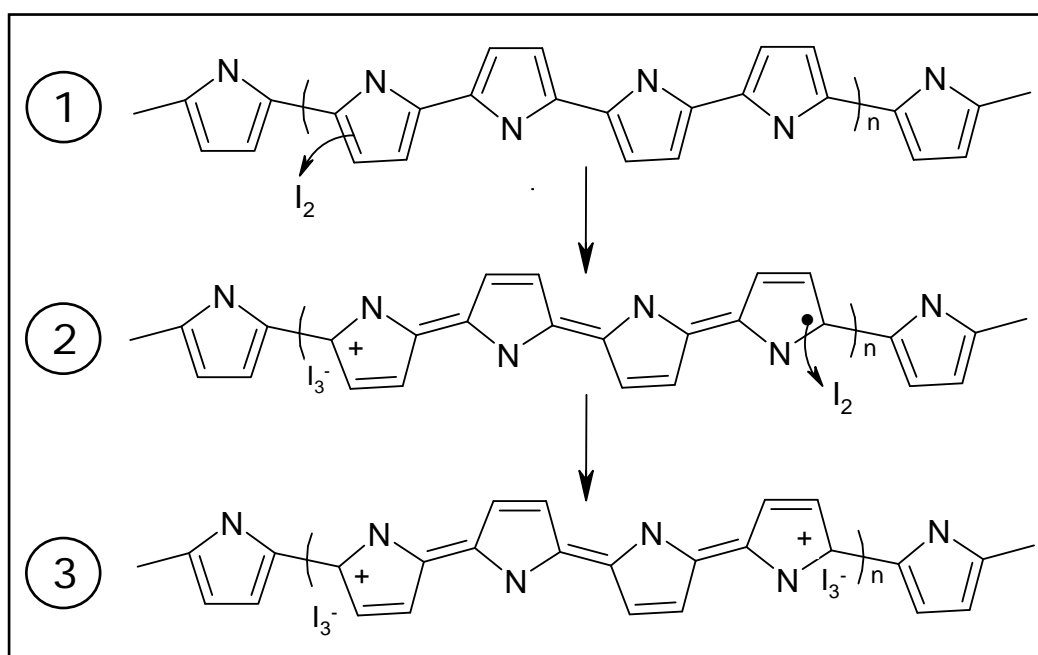

Figure 38. Transition from the reduced state (1) to the polaron state (2) and to the bipolaron state (3) in the polypyrrole doping process.

Furthermore, bipolarons not only participate in the intrachain conductivity but in the interchain as well. The mechanism proposed for conductivity between different polymeric chains is "charge hopping". That is, when electrons jump from a localized state to another on adjacent polymer chains and in this process, bipolarons help in exchange electrons from a neighbour polymeric chain.

3.6.2 EXPERIMENTAL PART

In order to carry out the doping process, PPy plasma polymerized films deposited on their respective substrate were introduced in a sealed saturated iodine chamber. The doping time varied from 5 to 60 min. After that, samples were placed under vacuum at 45 ºC for 30 min to remove all the unreacted iodine.

3.6.3 DOPING CHARACTERIZATION

3.6.3.1 Fourier Transform Infrared spectroscopy

FT-IR technique was used in order to characterize the incorporation of iodine as dopant agent in the plasma-polymerized PPy structure. Films synthesized exhibit characteristic vibrations of polypyrrole, as explained in previous section, plus characteristic vibrations of iodine. The absorption band for iodine doped plasma polymerized pyrrole appears at 1530 cm^{-1}.[27] Usually, PPy films tend to have some peaks around this wavelength. As a result, there is an enhancement of this absorption peak.

Figure 39 shows the FT-IR spectra of plasma PPy thin film deposited after 20 min of polymerization (blue line) and the same film iodine-doped for 20 (green line) and 60 (blue line) min with a 50% duty cycle (1s ON / 1s OFF). An intense peak for aromatic amines and a small peak for the C≡N group are seen at 3380 cm^{-1} and at 2200 cm^{-1}, respectively. Both peaks are characteristic of plasma synthesized PPy films. Moreover, a medium intense band is found around 1530 cm^{-1} for the non-doped sample. On the other hand, a very intense peak is observed at the same wavelength for the two other spectra, which had been iodine doped. Thereby, the observed increase in intensity of the absorption band stems from the incorporation of iodine within the polymer backbone.
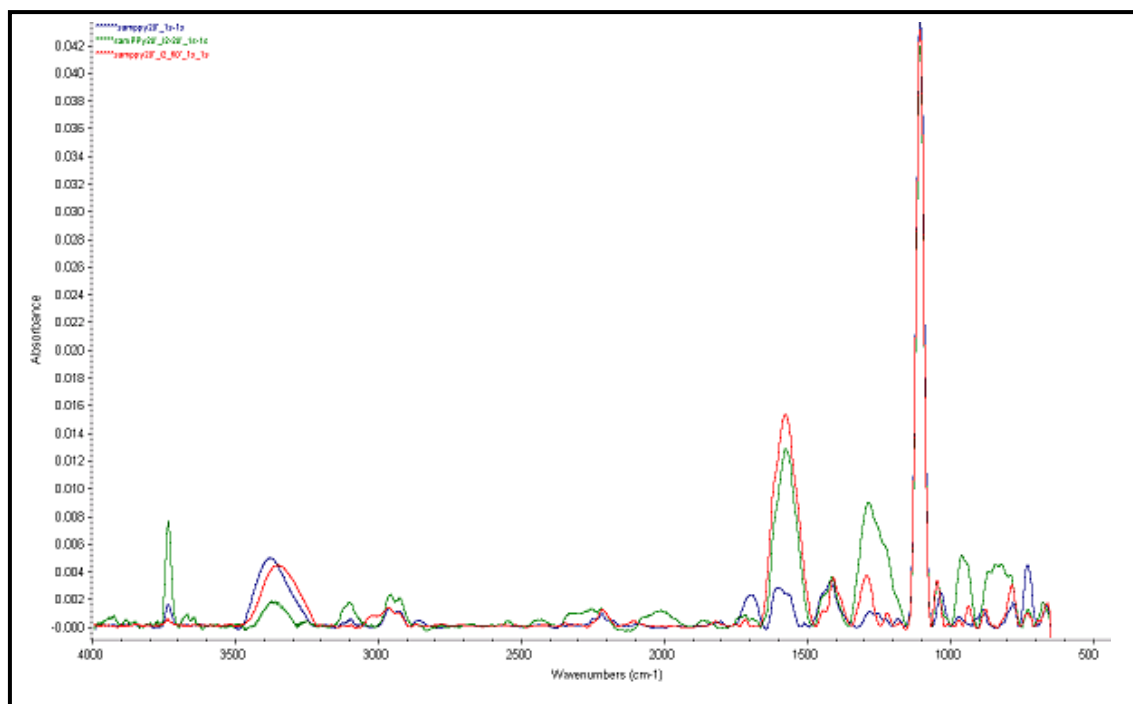
Figure 39. FT-IR spectra of plasma polymerized PPy thin films deposited after 20 min with a 50% duty cycle (1s ON / 1s OFF) (blue line) and iodine doped for 20 min (green line) and 60 min (red line).

Figure 40 displays other FT-IR spectra of plasma polymerized films deposited on SAM-modified silicon wafers after 5 min polymerization with a 90% duty cycle (orange line) and iodine doped for 20 min (red line) and 60 min (blue line). Because of the short polymerization time, the only characteristic absorption band of PPy intense enough appears at 3380 cm^{-1}, typical for secondary amines in the pyrrole ring. On the other hand, the two spectra which had been previously doped display an intense band at 1530 cm^{-1}, confirming again the incorporation of iodine in the structure. Moreover, the spectra indicate that iodine can diffuse easily through the PPy thin film regardless the thickness. The incorporation of iodine has been achieved in PPy plasma films polymerized for 5 and 20 min and FT-IR spectra have clearly shown the iodine absorption band for both samples.
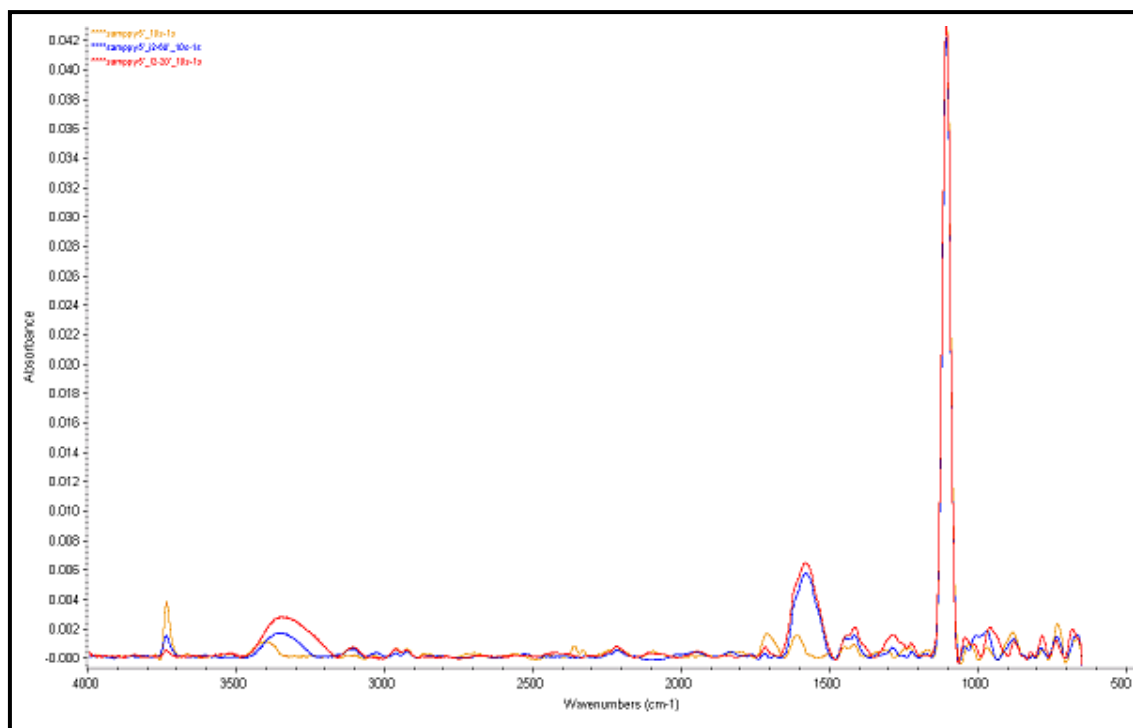
Figure 40. FT-IR spectra of plasma polymerized films on SAM-modified silicon wafers deposited after 5 min with a 90% duty cycle (orange line) and iodine doped for 20 min (red line) and 60 min (blue line).

3.6.3.2 XPS

To complete the surface study of the incorporation of iodine within the thin film, an XPS analysis was performed on the system. Figure 41 displays the XPS spectrum of a Py12SH SAM-modified copper substrate, polymerized for 1 min and iodine doped for 60 min. The survey spectrum consists of 5 peaks, three of them were found in pyrrole plasma polymerization: C 1s at 285 eV, N 1s at 400 eV and O 1s at 530 eV. In addition, two new peaks were detected at 620 and 630 eV corresponding to I $3d_{5/2}$ and I $3d_{3/2}$ signals respectively. Thereby, the iodine incorporation has also been identified in PPy thin films by XPS.
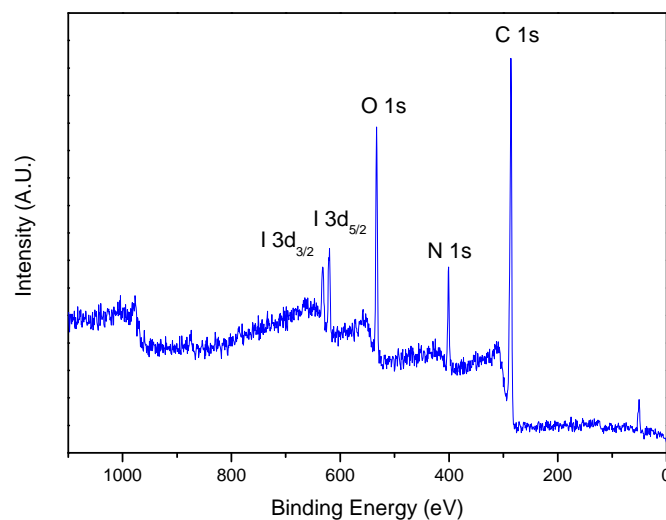
131

Figure 41. XPS spectrum of a Py12SH SAM-modified copper substrate, plasma polymerized for 1 minute and iodide doped for 60 min.

The surface composition of the different elements can be observed in Table 10. It should be noted that iodine is found in an appreciable concentration. Furthermore, the C/N, C/O and N/I ratios have been calculated and they are given in Table 11. The obtained C/N value (6.8) is higher in comparison with the C/N ratio for plasma polymerized films found in section 3.4.3.3 which was around 5 and the theoretical value for a polypyrrole film which is 4. The difference between doped and undoped samples could be correlated with the C/O ratio increase. The iodine doped film presents a C/O ratio of 4.2, whereas in the non-doped plasma polymerized films is 13. This means that a major amount of oxygen is found on the doped samples. The explanation for this might be related to the polymer chain oxidation helped by the exposure to iodine vapor. Because of this, the C/N ratio is a little bit higher than expected.

Another result that can provide valuable information is the N/I ratio. Assuming the bipolaron state model for iodine doped plasma polymerized PPy thin films as valid, the theoretical N/I ratio should be 2. Each four pyrrole units, there are two positive charges on the polypyrrole backbone. Therefore, to compensate these two charges two iodide anions are place next to them. Then, each four nitrogen atoms, there are two iodine atoms. The obtained ratio for our samples is 2.5, which is quite close to the theoretical value. Taking in account that plasma polymerization result in a new kind of material, whose structure is different from the obtained by other conventional techniques, it can be considered that the doping process has been carried out properly.

Table 10. Surface composition of Py12SH SAM-modified copper substrate, plasma polymerized for 1 minute and iodide doped for 60 min.

	PPy1m/I_2
	Py12SH
C (1s)	69.3
N (1s)	10.1
O (1s)	16.6
I (3d)	4.0

Table 11. C/N, C/O and N/I ratios of Py12SH SAM-modified copper substrate, plasma polymerized for 1 minute and iodide doped for 60 min.

	PPy1m/I_2
	Py12SH
C/N	6.8
C/O	4.2
N/I	2.5

XPS deconvolution

The doping process involves nitrogen oxidation within the polymer backbone. This change in the chemical state of nitrogen can be studied by high resolution XPS. Therefore, Figure 42 shows the deconvolution of the N 1s XPS spectra of a Py12SH SAM-modified copper, polymerized for 1 min and iodine doped for 60 min. The signal has been splitted into 4 peaks. The peak at 401.5 eV has been assigned to the oxidized pyrrole specie, -N^+-,[31] the peak at 400 eV corresponds to the neutral nitrogen, C-N, the peak at 398.6 eV to the C=N bond and the peak at 397.2 eV to the C≡N bond. The -N^+- group was not found in the plasma polymerized PPy, since it is obtained in its reductive (non-conducting) form and only after polymer oxidation the -N^+- group appears. Table 12 presents the chemical composition of the deconvoluted N 1s signal. The strongest peak corresponds to the C-N bond and the ratio between -N^+- and N is 15%. Kim *et al*[39] reported a proportion of positively charged nitrogen within the range of 25-30% for chemically synthesized PPY doped with sodium dodecylbenzenosulfonate, which value has been taken as a reference. Wang *et al*[27] achieved a –N^+-/N ratio between 20 and 25% for plasma synthesized PPy films doped with I_2. The result found in our research is about 15%, which is quite close to ones obtained in the literature. Thus, that indicates a good quality either in the PPy deposition and the doping process.
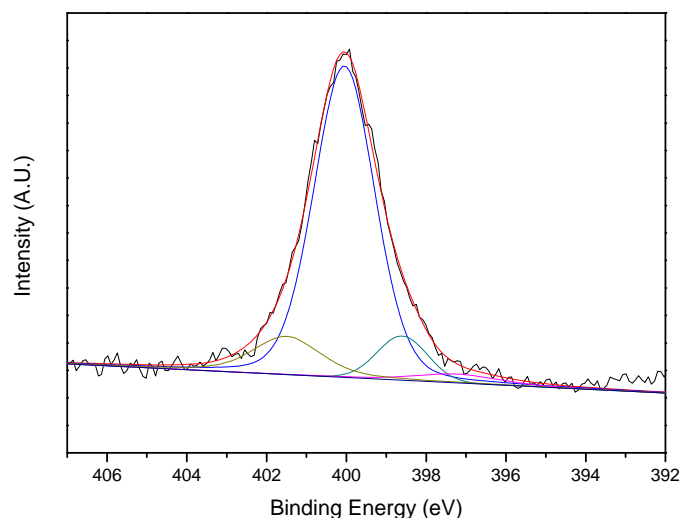
Figure 42. High resolution N 1s Xps spectrum of Py12SH SAM assembled on copper, polymerized for 1min and iodine doped for 60 min.

Table 12. Chemical composition (%) of the deconvoluted N 1s signal for Py12SH SAM-modified copper, plasma polymerized for 1 min and iodine doped for 60 min.

		PPy1m/I$_2$
Bond	Energy Binding (eV)	Py12SH
-N$^+$-	401.5	11.9
C-N	400.0	79.3
C=N	398.6	5.4
C≡N	397.2	3.4

The deconvoluted XPS spectrum of the C 1s signal is provided in Figure 43. The signal has been divided into three peaks corresponding to C-N, C=N and C≡N functionalities at binding energies of 284.8, 286.0 and 288.0 eV and their composition can be observed in Table 13. The C-C peak shows the strongest peak as it was commented in plasma polymerization section. Furthermore, the C≡N functionality in the iodine doped sample has showed an important increase in comparison with the plasma polymerization of pyrrole. The observed increase could be attributed to a higher amount of oxygen found in the XPS analysis. The iodine doped film presents a C/O ratio of 4.2, while in the plasma polymerization is 13. Therefore, the C≡N increase may be explained by the fact that the deconvoluted peak do not correspond only to the C≡N functionality but the sum of this one and several oxidized species. This interpretation is corroborated by the deconvoluted N 1s spectrum, in which the nitrogen belonging to C≡N was observed in a low concentration. As a consequence, the carbon peak of this bond can not be so strong in the deconvoluted C 1s signal by itself. It has been

134

reported that C=O and O=C-NH functionalities appear at 287.8 eV. These two groups may be perfectly present in the PPy backbone and because their binding energy is very close to the C≡N one, it would be impossible trying to distinguish among them. Thereby, the C≡N peak is, indeed, the result of several chemical state contributions. The resulting oxidized functionalities can be created by the polymer introduction into an oxidative iodine atmosphere and a longer exposure to air.
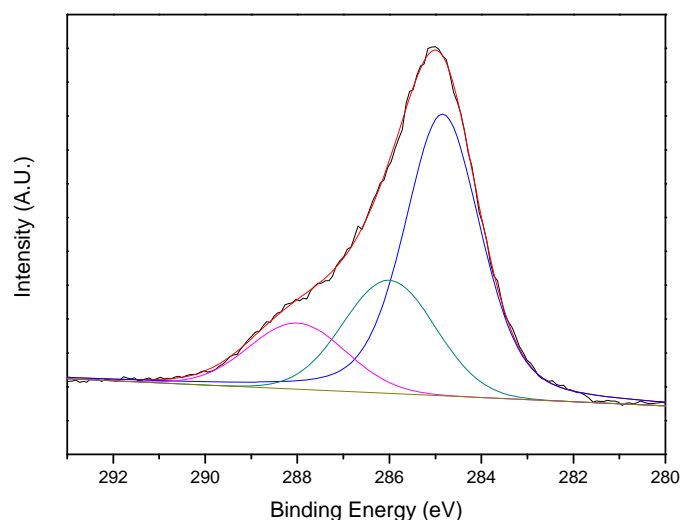

Figure 43. High resolution C 1s XPS spectrum of Py12SH SAM assembled on copper, polymerized for 1min and iodine doped for 60 min.

Table 13. Chemical composition (%) of the deconvoluted C 1s signal for Py12SH SAM-modified copper, plasma polymerized for 1 min and iodine doped for 60 min.

		PPy1m/I$_2$
Bond	Energy Binding (eV)	Py12SH
C-C	284.8	70.3
C=N	286.0	11.7
C≡N	288.0	18.0

3.6.3.3 Atomic Force Microscopy

The surface topography of a plasma synthesized PPy thin film and iodine doped is shown in Figure 44. This sample corresponds to the same displayed in Figure 31 plus an iodine doping process of 40 minutes. Both of them present the same structure: a PPy film with globules on top of it. Nevertheless, iodine vapour exposure has lead to a change in the topography. In this case, the AFM 3D images give very valuable information about the modification involved in the doping process. The main difference observed is the surface roughness. Figure 31 shows a flat surface, whereas in Figure

44 there have appeared like small peaks at ground level, which makes a more irregular surface. The RMS roughness for the sample plasma polymerised for 20 min is 7.7 nm and for the sample polymerised for 20 min and iodine doped for 40 min is 21.1 nm. The roughness increase is owed to the iodine incorporation within the polymer backbone. The inclusion of the iodine necessarily must affect the polymer surface topography.
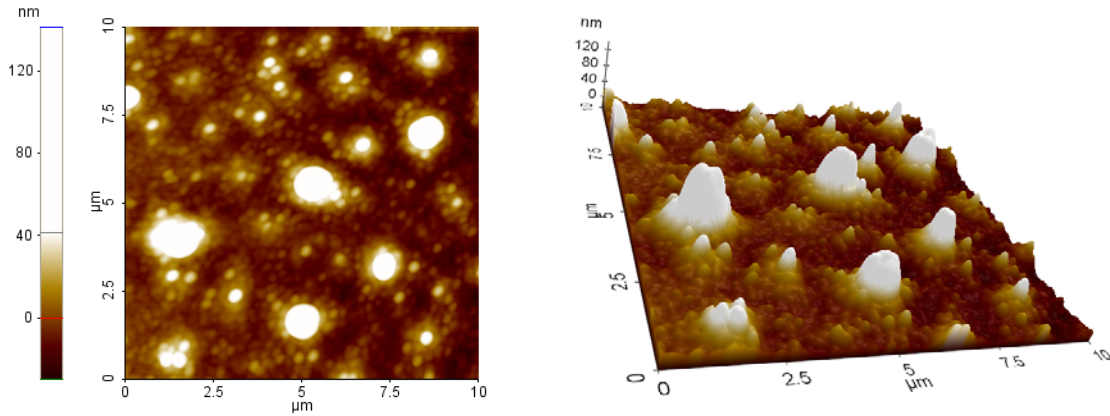

Figure 44. 2D (left side) and 3D (right side) AFM topography images of a PPy thin film plasma polymerized for 20 min on copper and iodine doped for 40 min.
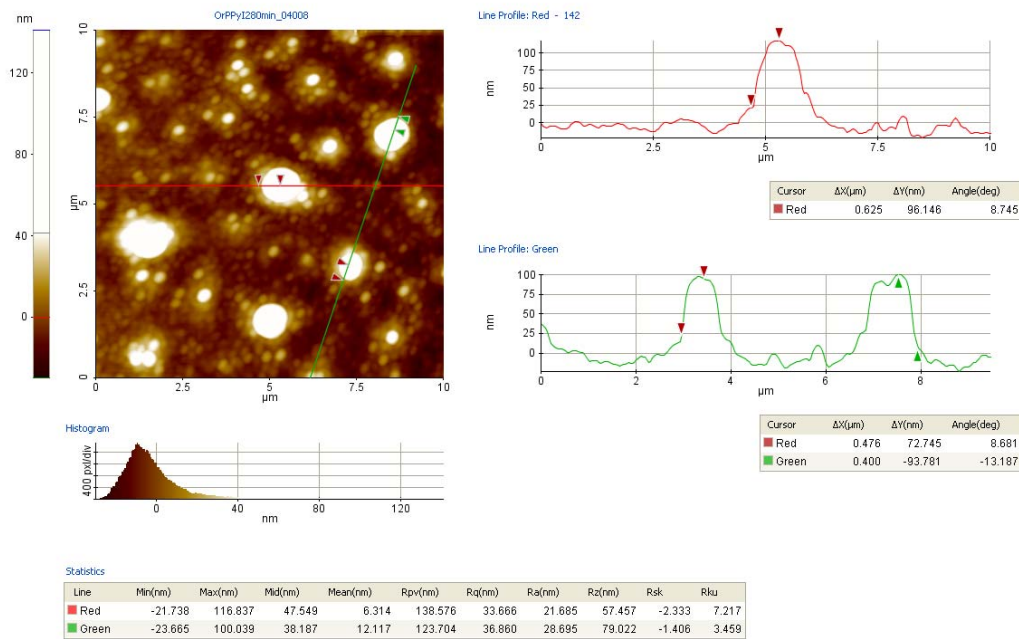

Figure 45. Line profile of an AFM image of a PPy thin film plasma polymerized for 20 min on copper and iodine doped for 40 min.

Line profile analysis in Figure 45 shows that globules height measure between 70 and 100 nm, which are higher than peaks measured in Figure 32. This can be attributed to the iodine incorporation as well, and it gives unquestionable evidence that the doping process affects the polymer morphology.

136

3.7 REFERENCES

1. Bradley, A.; Hammes, J. P. Electrical Properties of Thin Organic Films. *J. Electrochem. Soc.* **1963,** *110* (1), 15-22.

2. Bradley, A. Organic Polymer Coating Deposited from A Gas Discharge. *Industrial & Engineering Chemistry Product Research and Development* **1970,** *9* (1), 101.

3. Goodman, J. The Formation of Thin Polymer Films in the Gas Discharge. *Journal of Polymer Science* **1960,** *44* (144), 551-552.

4. Maier, G. Low dielectric constant polymers for microelectronics. *Progress in Polymer Science* **2001,** *26* (1), 3-65.

5. Coulson, S. R.; Woodward, I. S.; Badyal, J. P. S.; Brewer, S. A.; Willis, C. Ultralow Surface Energy Plasma Polymer Films. *Chem. Mater.* **2000,** *12* (7), 2031-2038.

6. Merlo, J. A.; Newman, C. R.; Gerlach, C. P.; Kelley, T. W.; Muyres, D. V.; Fritz, S. E.; Toney, M. F.; Frisbie, C. D. p-Channel Organic Semiconductors Based on Hybrid AceneᴦêÆThiophene Molecules for Thin-Film Transistor Applications. *J. Am. Chem. Soc.* **2005,** *127* (11), 3997-4009.

7. Xie, X.; Thiele, J. U.; Steiner, R.; Oelhafen, P. Preparation and characterization of conducting plasma polymers of tetracyanoquinodimethane (TCNQ) with quinoline. *Synth. Met.* **1994,** *63* (3), 221-224.

8. Inagaki, N.; Tasaka, S.; Ikeda, Y. Plasma Polymerization of Copper Phthalocyanines and Application of the Plasma Polymer-Films to No2 Gas Sensor Device. *J. Appl. Polym. Sci.* **1995,** *55* (10), 1451-1464.

9. Muguruma, H.; Karube, I. Plasma-polymerized films for biosensors. *TrAC Trends in Analytical Chemistry* **1999,** *18* (1), 62-68.

10. Yasuda, H. *Luminous Chemical Vapor Deposition and Interface Engineering;* Marcel Dekker: New York, **2005**.

11. Borros, S.; Diago, M. P.; Esteve, J.; Agullo, N. Structural and morphological differences of thin films obtained by plasma polymerization of pyrrole (Ppy) and thiophene (Pth). *Materials Research Society Symposia Proceedings 725[Organic and Polymeric Materials and Devices--Optical, Electrical and Optoelectronic Properties]* **2002,** 225-230.

12. Martin, L.; Esteve, J.; Borros, S. Growth vs. nucleation of conducting polymers thin films obtained by plasma-enhanced chemical vapor deposition. *Thin Solid Films* **2004,** *451-52*, 74-80.

13. Yasuda, H.; Hsu, T. Some Aspects of Plasma Polymerization Investigated by Pulsed Rf Discharge. *Journal of Polymer Science Part A-Polymer Chemistry* **1977,** *15* (1), 81-97.

14. Willicut, R. J.; Mccarley, R. L. Electrochemical Polymerization of Pyrrole-Containing Self-Assembled Alkanethiol Monolayers on Au. *J. Am. Chem. Soc.* **1994,** *116* (23), 10823-10824.

15. Willicut, R. J.; Mccarley, R. L. Surface-Confined Monomers on Electrode Surfaces - Electrochemical and Microscopic Characterization of Omega-(N-Pyrrolyl)Alkanethiol Self-Assembled Monolayers on Au. *Langmuir* **1995,** *11* (1), 296-301.

16. Doron-Mor, I.; Barkay, Z.; Filip-Granit, N.; Vaskevich, A.; Rubinstein, I. Ultrathin gold island films on silanized glass. Morphology and optical properties. *Chem. Mater.* **2004,** *16* (18), 3476-3483.

17. Zhang, L.; Cosandey, F.; Persaud, R.; Madey, T. E. Initial growth and morphology of thin Au films on TiO2(110). *Surf. Sci.* **1999,** *439* (1-3), 73-85.

18. Bumm, L. A.; Arnold, J. J.; Dunbar, T. D.; Allara, D. L.; Weiss, P. S. Electron transfer through organic molecules. *Journal of Physical Chemistry B* **1999,** *103* (38), 8122-8127.

19. Wu, C. G.; Chiang, S. C.; Wu, C. H. Formation and electrochemical property of pyrrole-terminated SAMs and the effect of the SAMs on the physicochemical properties of polypyrrole films electrochemically deposited over them. *Langmuir* **2002,** *18* (20), 7473-7481.

20. Cen, L.; Neoh, K. G.; Kang, E. T. Surface functionalization of electrically conductive polypyrrole film with hyaluronic acid. *Langmuir* **2002,** *18* (22), 8633-8640.

21. Van Ooij, W. J.; Luo, S.; Datta, S. Surface modification of textile fibers and cords by plasma polymerization. *Plasmas Polym.* **1999,** 4(1), 33-55.

22. Wittmer, J. P.; Cates, M. E.; Johner, A.; Turner, M. S. Diffusive growth of a polymer layer by in situ polymerization. *Europhys. Lett.* **1996,** *33* (5), 397-402.

23. Hearn, M. J.; Fletcher, I. W.; Church, S. P.; Armes, S. P. Characterization of Polypyrrole Fiber Composites by Time-Of-Flight Secondary Ion Mass-Spectrometry and Vibrational Spectroscopy. *Polymer* **1993,** *34* (2), 262-266.

24. Abel, M. L.; Chehimi, M. M.; Brown, A. M.; Leadley, S. R.; Watts, J. F. Adsorption-Isotherms of Pmma on A Conducting Polymer by Tof-Sims. *J. Mater. Chem.* **1995,** *5* (6), 845-848.

25. Lascelles, S. F.; Armes, S. P.; Zhdan, P. A.; Greaves, S. J.; Brown, A. M.; Watts, J. F.; Leadley, S. R.; Luk, S. Y. Surface characterization of micrometre-sized, polypyrrole-coated polystyrene latexes: verification of a 'core-shell' morphology. *J. Mater. Chem.* **1997,** *7* (8), 1349-1355.

26. Abel, M. L.; Leadley, S. R.; Brown, A. M.; Petitjean, J.; Chehimi, M. M.; Watts, J. F. Tof-Sims Characterization of Electrochemically Synthesized Polypyrrole Films. *Synth. Met.* **1994,** *66* (1), 85-88.

27. Wang, J. G.; Neoh, K. G.; Kang, E. T. Comparative study of chemically synthesized and plasma polymerized pyrrole and thiophene thin films. *Thin Solid Films* **2004,** *446* (2), 205-217.

28. vanOoij, W. J.; Guo, S. DC plasma polymerization of pyrrole and hexamethyldisiloxane: Mechanisms, characterization and applications. *Abstracts of Papers of the American Chemical Society* **1997,** *213*, 457.

29. Takai, O.; Anita, V.; Saito, N. Properties of DLC thin films produced by RF PE-CVD from pyrrole monomer. *Surf. Coat. Technol.* **2005,** *200* (1-4), 1106-1109.

30. Eufinger, S.; vanOoij, W. J.; Ridgway, T. H. DC plasma-polymerization of pyrrole: Comparison of films formed on anode and cathode. *J. Appl. Polym. Sci.* **1996,** *61* (9), 1503-1514.

31. Suzer, S.; Birer, O.; Sevil, U. A.; Guven, O. XPS investigations on conducting polymers. *Turkish Journal of Chemistry* **1998,** *22* (1), 59-65.

32. Sahin, H. T. Pyrrole thin films deposited on paper by pulsed RF plasma. *Central European Journal of Chemistry* **2007,** *5* (3), 824-834.

33. Yang, P.; Zhang, J.; Guo, Y. Synthesis of intrinsic fluorescent polypyrrole nanoparticles by atmospheric pressure plasma polymerization. *Appl. Surf. Sci.* **2009,** *255* (15), 6924-6929.

34. D.B.Cairns; S.P.Armes . X-ray Photoelectron Spectroscopy Characterization of Sbmicrometer-Sized Polypyrrole-Polystyrene Composites. *Langmuir* **1999,**15, 8059-8066.

35. Jaramillo, A.; Spurlock, L. D.; Young, V.; Brajter-Toth, A. XPS characterization of nanosized overoxidized polypyrrole films on graphite electrodes. *Analyst* **1999,** *124* (8), 1215-1221.

36. Han, L. M.; Timmons, R. B.; Bogdal, D.; Pielichowski, J. Ring retention via pulsed plasma polymerization of heterocyclic aromatic compounds. *Chem. Mater.* **1998,** *10* (5), 1422-1429.

37. Cioffi, N.; Torsi, L.; Losito, I.; Di Franco, C.; De Bari, I.; Chiavarone, L.; Scamarcio, G.; Tsakova, V.; Sabbatini, L.; Zambonin, P. G. Electrosynthesis and analytical characterisation of polypyrrole thin films modified with copper nanoparticles. *J. Mater. Chem.* **2001,** *11* (5), 1434-1440.

38. Shirakawa, H.; Louis, E. J.; Macdiarmid, A. G.; Chiang, C. K.; Heeger, A. J. Synthesis of Electrically Conducting Organic Polymers - Halogen Derivatives of Polyacetylene, (Ch)X. *Journal of the Chemical Society-Chemical Communications* **1977,** (16), 578-580.

39. Kim, I. W.; Lee, J. Y.; Lee, H. Solution-cast polypyrrole film: the electrical and thermal properties. *Synth. Met.* **1996,** *78* (2), 177-180.